Geologica Acta, Vol.15, Nº 4, December 2017, 409-428, I-VIII
DOI: 10.1344/GeologicaActa2017.15.4.10

geologica acta

Coeval interaction between magmas of contrasting composition (Late Carboniferous-Early Permian Santa Eulália-Monforte massif, Ossa-Morena Zone): field relationships and geochronological constraints

M. F. PEREIRA[1] C. GAMA[1] C. RODRÍGUEZ[2]

[1]Instituto de Ciências da Terra, Departamento de Geociências, ECT, Universidade de Évora
Rua Romão Ramalho 59, 7000-671, Évora, Portugal. Pereira E-mail: mpereira@uevora.pt
Gama E-mail: cgama@uevora.pt

[2]Departamento de Ciencias de la Tierra, Universidad de Huelva
Huelva, Spain. Rodríguez E-mail: carmen.rodriguez@dgeo.uhu.es

ABSTRACT

The Santa Eulália-Monforte massif is a post-kinematic Late Carboniferous-Early Permian calc-alkaline composite massif (LC-EP) located in the Ossa-Morena Zone (OMZ, Portugal). This paper examines the field relationships between pinkish granites and mafic-intermediate rocks from the external ring of this massif and presents new U-Pb zircon age determinations. The estimated $^{206}Pb/^{238}U$ ages, 297±4Ma for the pinkish granite and 303±3Ma for a gabbro-diorite point to a short time interval between the crystallization of both magmas. At outcrop scale, contacts of the mafic-intermediate rocks with the host pinkish granite are sharp and corroborate this age relationship, but do not justify why the host-enclave contacts often has curved and irregular shapes, indicating liquid-liquid interaction. A full analysis of the distribution of U-Pb zircon ages and respective Th/U ratios suggests that the compositionally distinct magmas were roughly contemporaneous. The obtained ages also fit the LC-EP Iberian calc-alkaline suite that was formed contemporaneously to the development of the Iberian-Armorican Arc and when the Paleotethyan oceanic Plate subducted under the Eurasian active margin. Taking this geodynamic setting as a reference, the LC-EP Iberian calc-alkaline magmatism can be interpreted as most probably related to the Cimmerian cycle instead of the traditionally accepted model that ascribe a closer connection of this magmatism with the Variscan cycle.

KEYWORDS | **Iberian Massif. Late Carboniferous-Early Permian. Calc-alkaline bimodal plutonism. Zircon dating. Variscan and Cimmerian cycles.**

INTRODUCTION

The Iberian Massif experienced a polymetamorphic evolution during the Carboniferous as a result of the collision between Laurussia and Gondwana (*e.g.* Variscan Orogeny; Martínez Catalán *et al.*, 2009; Díez Fernández *et al.*, 2016). The Laurussia-Gondwana convergence caused crustal thickening by the stacking of tectonic nappes and the rejuvenation of reliefs. The regional switch from contractional to extensional deformation was followed by an orogenic collapse and the generation of abundant crustal-derived magmatism (Escuder Viruete

et al., 1994; Pereira *et al*., 2009; 2017a; Martínez Catalán *et al*., 2014; Alcock *et al*., 2015; Cambeses *et al*., 2015; Díez Fernández and Pereira, 2016). Mantle contributions were more abundant towards the SW Iberian Massif, as syn-kinematic magmatism related to intra-orogenic extension was slightly older in the Ossa-Morena and South Portuguese zones (Simancas *et al*., 2005; Pereira *et al*., 2009; 2015a) than in the Central Iberian Zone.

The age and compositional ranges of syn-kinematic (Carboniferous) and post-kinematic (Late Carboniferous-Early Permian, LC-EP) intrusions are wide in the NW (*e.g*. Central Iberian Zone; Castro *et al*., 2002 and references therein) and SW (Ossa-Morena Zone; Pereira *et al*., 2015a and references therein) Iberian Massif. Most syn- and post-kinematic granitic rocks are S-type peraluminous, but there are also granitic rocks with transitional features between S- and I-type, I-type granites and hybrid granites, including metaluminous varieties (Dias *et al*., 1998, 2002; Castro *et al*., 1999, 2002; Bea *et al*., 1999, 2003; Fernández-Suárez *et al*., 2000, 2011; Neiva and Gomes 2001; González Menéndez *et al*., 2006; Moita *et al*., 2009; Neiva *et al*., 2009; Solá *et al*., 2009; Lima *et al*., 2011, 2012; Teixeira *et al*., 2011; Villaseca *et al*., 2012; Merino Martínez *et al*., 2014; Pereira *et al*., 2015a, 2017a; LópezMoro *et al*., 2017). These Carboniferous and Permian calc-alkaline granitic rocks are often closely and spatially associated with calc-alkaline mafic-intermediate rocks (*e.g*. Castro *et al*., 2003; Bea, 2004; Larrea *et al*., 2004; González Menéndez *et al*., 2006; Jesus *et al*., 2007; Pin *et al*., 2008; Solá *et al*., 2009; Moita *et al*., 2015) and are characterized by many structures and textures formed through the complex interplay of distinct petrogenetic processes. Such composite plutons typically preserve an integrated record of prolonged magmatic evolution, including pluton accumulation, crystallization and emplacement within the crust that evidence the coeval interaction between two or more magmas of contrasting composition and physical properties (Turnbull *et al*., 2010). Mixing of magmas within a magma chamber to produce a homogeneous hybrid, followed by mingling and partial mixing of the hybrid magma with one of the remaining end-members is commonly identified in the successive stages of the magmatic history of composite plutons (Barbarin, 2005 and references therein). By studying the temporal and spatial interaction of magmas of contrasting compositions that remained in the contact in liquid state, insights can be gained into the duration of physical and thermal processes responsible for the formation of plutons.

Our study presents original field data and SHRIMP zircon U-Pb dating for a post-kinematic intrusion in the Ossa-Morena Zone with the aim of studying the temporal and spatial interaction of a felsic and a mafic-intermediate magma forming the external ring of the Santa Eulália-Monforte massif. The obtained results will shed light on the timing of crystallization and emplacement of the Santa Eulália-Monforte intrusion, and on the global geodynamic context of the post-kinematic Iberian calc-alkaline magmatism. The results achieved broaden the knowledge on the spatial and temporal relationships between distinct LC-EP post-kinematic intrusions of the Iberian Massif. Our data also show that the crystallization ages of the Santa Eulália-Monforte I-type granite and associated mafic rocks are younger than the Nisa-Albuquerque batholith. Both intrusions cut across the Variscan structures, establishing a maximum range of about 13Ma, from the Late Moscovian to Asselian, for the LC-EP post-kinematic magmatism in the SW Iberian Massif. The subject of this study was chosen because L.G. Corretgé, who receives an honorable mention in this volume, was one of the petrologists who mostly contributed to gather data on the magmatism of the Iberian Massif, thus, fostering scientific cooperation between Portuguese and Spanish geologists.

LP-EC POST-KINEMATIC INTRUSIONS OF THE IBERIAN MASSIF

The LC-EP granitic rocks of the Iberian Massif have been traditionally classified as Late-Variscan because they crosscut the main Variscan structures and syn-kinematic intrusive rocks (*ca*. 306-287Ma; Ferreira *et al*., 1987; Dias *et al*., 1998; Fernández-Suárez *et al*., 2011; Neiva *et al*., 2012; Orejana *et al*., 2012; Villaseca *et al*., 2012). However, these post-kinematic intrusions are also recently considered as unrelated to the Gondwana-Laurussia collision *sensu stricto* (*e.g*. Gutiérrez-Alonso *et al*., 2011; Pereira *et al*., 2015b).

The LC-EP post-kinematic intrusions are abundant in the Central Iberian Zone, but are relatively less represented in the Ossa-Morena Zone. The Nisa-Albuquerque massif is a composite elongated body oriented parallel to, and crossing, the boundary between the Central Iberian and Ossa-Morena zones (González Menéndez, 2002) (Fig. 1). This post-kinematic intrusion consists of a dominant S-type monzogranite-syenogranite (*ca*. 309-307Ma) that surrounds a discontinuous core of I-type tonalite-granodiorite (*ca*. 306Ma) (SHRIMP zircon U-Pb dating; Solá *et al*., 2009). The Santa Eulália-Monforte massif, located in the northern domains of the Ossa-Morena Zone, is a composite intrusion (Gonçalves and Coelho, 1969-1970; Gonçalves, 1971; Gonçalves *et al*., 1972, 1975; Carrilho Lopes *et al*., 1998; Sant'Ovaia *et al*., 2015) consisting of S- and I-type granites and mafic-intermediate bodies (González Menéndez *et al*., 2006). Rb-Sr whole-rock ages of *ca*. 281Ma (Mendes, 1967-1968) and of *ca*. 290Ma (Pinto *et al*., 1987) have been, for decades, the only available isotopic ages performed on granites from the Santa Eulália-Monforte massif.

THE SANTA EULÁLIA-MONFORTE MASSIF

Host rocks of the Santa Eulália-Monforte massif

The Santa Eulália-Monforte massif intrudes two important domains of the Ossa-Morena Zone (Figs. 1 and 2): i) the strongly deformed and variable metamorphosed Ediacaran to Ordovician sedimentary and igneous rocks of the Coimbra-Córdoba shear zone (Burg *et al.*, 1981; Pereira *et al.*, 2008, 2010); and ii) the Cambrian-Ordovician sedimentary and igneous rocks of the Alter do Chão-Elvas sector (Apalategui *et al.*, 1990; Oliveira *et al.*, 1991).

The original contacts and textures of the Ediacaran-Cambrian sedimentary and volcanic rocks (Pereira *et al.*, 2006; Linnemann *et al.*, 2008) and Cambrian-Ordovician plutonic rocks (Pereira *et al.*, 2011; Sánchez-García *et al.*, 2013; Díez Fernández *et al.*, 2015) are best exposed in the northern and southern margins (Fig. 2). In the northern and southern margins of the Coimbra-Córdoba shear zone, as well as in the Alter do Chão-Elvas sector, despite the Variscan ductile deformation and greenschist facies metamorphism, the Ediacaran succession-consisting of metapelite, metagreywacke, black metachert, metamafic rocks, and rare carbonate rocks is unconformably overlain by a Cambrian sequence (Gonçalves, 1971; Gonçalves *et al.*, 1975; Oliveira *et al.*, 1991; Pereira *et al.*, 2006). From the base to the top, the Cambrian sequence consists of: i) felsic metavolcanic rocks, quartzite and marble, and ii) schists, metagreywackes, quartzites, metaconglomerates and metamafics rocks. Cambrian magmatism includes calc-alkaline and MORB compositions (Pereira and Quesada, 2006; Sánchez-García *et al.*, 2010). The Ediacaran-Cambrian succession is intruded by Cambrian-Ordovician peralkaline and alkaline igneous rocks (Gonçalves and Assunção, 1970; Gonçalves *et al.*, 1975: Díez Fernández *et al.*, 2015).

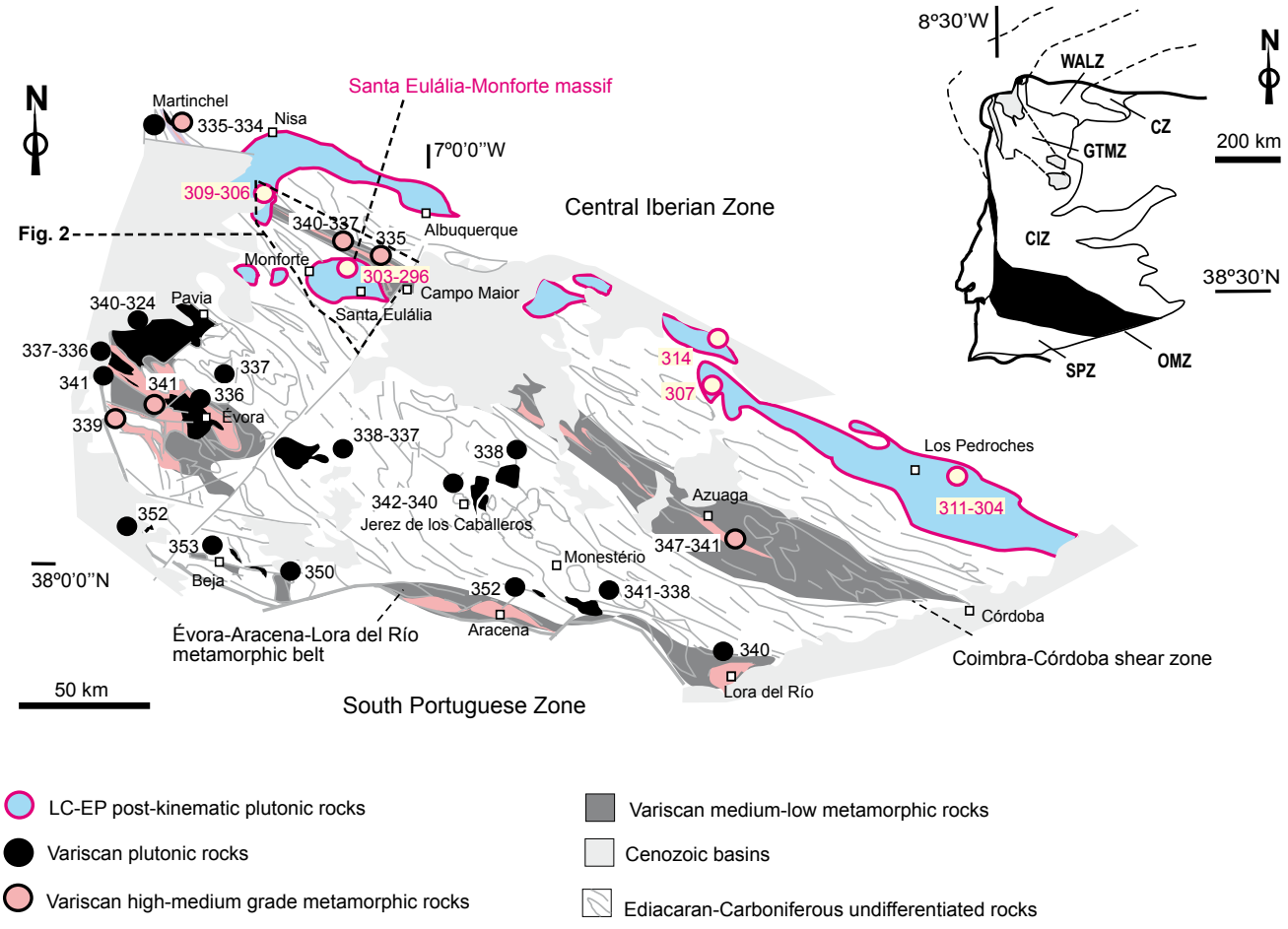

FIGURE 1. Schematic geological map of the Ossa-Morena Zone, showing the location of the Variscan plutonic and metamorphic rocks (adapted from Pereira *et al.*, 2015a and references therein), and the Late Carboniferous-Early Permian (LC-EP) post-kinematic plutonic rocks, including the Santa Eulália-Monforte Massif. Inset of the main subdivision of the Évora Massif: CIZ: Central Iberian Zone; CZ: Cantabrian Zone; GTMZ: Galicia-Trás-os-Montes Zone; OMZ: Ossa-Morena Zone; SPZ: South Portuguese Zone; WALZ: West Asturian-Leonese Zone.

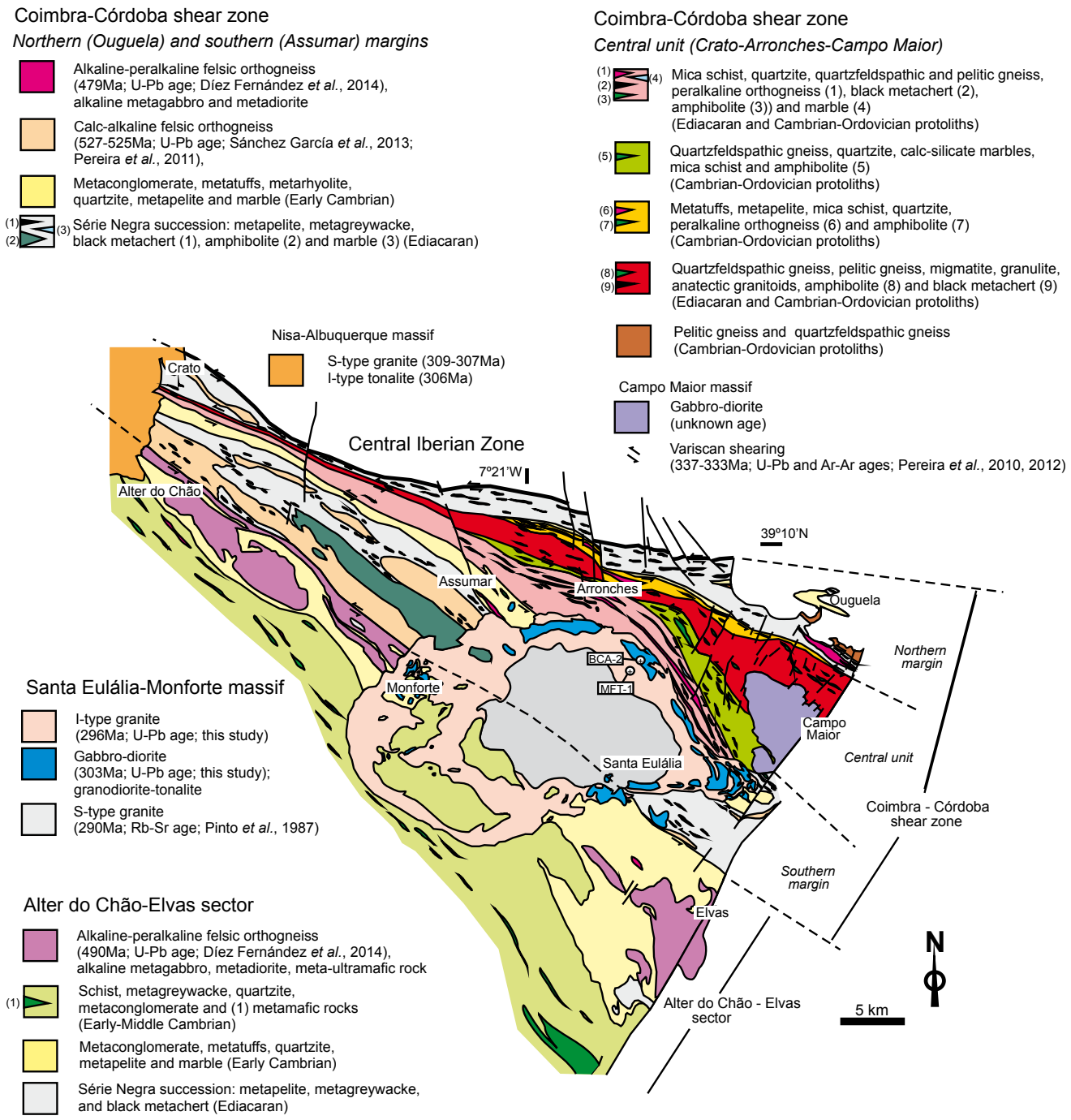

FIGURE 2. Geologic map of the northern domains of the Ossa-Morena Zone (Portugal) (adapted from Gonçalves and Assunção, 1970; Gonçalves, 1971; Gonçalves *et al.*, 1972, 1975; Gonçalves and Fernandes, 1973; Pereira, 1999; Pereira *et al.*, 2008, 2010), including the Santa Eulália-Monforte massif intrusive in the Coimbra-Córdoba shear zone and in the Alter do Chão-Elvas sector. Sample locations (BCA-2 and MFT-1) are shown.

In the Central Unit of the Coimbra-Córdoba shear zone, the Carboniferous (*ca.* 340-333Ma) ductile deformation and associated metamorphism, reaching amphibolite to granulite and ecologite facies conditions, transformed the original contact and textures of the Ediacaran-Ordovician rocks (Pereira *et al.*, 2008, 2010, 2012) (Fig. 2). Cambrian-Ordovician plutons occur as elongated bodies of weakly- to moderately-foliated rocks, or as narrow bands of orthogneiss alternating with schists and paragneisses affected by strong Variscan deformation and metamorphism (Gonçalves *et al.*, 1972; Pereira *et al.*, 2008, 2010; Díez Fernández *et al.*, 2015) (Fig. 1).

Field relationships, petrography and geochemistry

The Santa Eulália-Monforte massif (Fig. 2) is a ring-shaped composite intrusion 18km wide and 32km long elongated body in E-W direction (Gonçalves and Coelho, 1969-1970; Gonçalves, 1971; Gonçalves *et al.*, 1972, 1975; Oliveira, 1975; Carrilho Lopes *et al.*, 1998; González Menéndez *et al.*, 2002, 2006). It includes a 10km wide and 16km long core of greyish fine- to medium-grained biotite granite (Fig. 3A) surrounded by a ring consisting of a complex association between pinkish coarse-grained biotite granite and mafic-intermediate rocks (Figs. 3, 4, 5 and 6).

The core of this ring-shaped intrusion consists of S-(prevailing) and I-type high-K calc-alkaline peraluminous granite ranging in composition from monzogranite to granite (Fig. 7A; B). Quartz, plagioclase, microcline, biotite and muscovite are the main minerals, being also present cordierite (Fig. 3A). The geochemistry of the greyish granite suggests the derivation from a mixed source of metasedimentary (dominant) with intermediate to acid igneous rocks extracted from the mid-lower crust (González Menéndez *et al.*, 2006). The external pinkish granite is composed of quartz, biotite, and K-feldspar prevails in respect to plagioclase. It also contains chlorite, amphibole, allanite and zircon. The available geochemical data (Carrilho Lopes *et al.*, 1998; González Menéndez *et al.*, 2006) indicate that it is an I-type high-K calc-alkaline peraluminous granite (Fig. 7A; C). The pinkish granite is interpreted to derive from partial melting of intermediate composition gneissic rocks from the mid-lower crust (González Menéndez *et al.*, 2006).

The pinkish granite of the external ring (Fig. 6A) includes variable size and irregular, 0.5-1.5km wide and 0.8-6km long gabbro-diorite to granodiorite-quartzdiorite-tonalite enclaves, and kilometer-scale xenoliths consisting of Ediacaran and Cambrian host rocks (Fig. 6B). Mafic-intermediate rocks range compositionally (Fig. 7) from gabbro-diorite, which are mainly composed by plagioclase, amphibole, pyroxene, biotite, apatite and zircon, to granodiorite-quartzdiorite-tonalite consisting of plagioclase, K-feldspar, quartz, biotite, amphibole, apatite and zircon. The mafic-intermediate associations have been interpreted to derive from distinct sources (González Menéndez *et al.*, 2006): an enriched mantle (gabbro-diorite) and from partial melting of a lower mafic crust (granodiorite-quartzdiorite-tonalite).

Field relationships show that the greyish granite from the core (Fig. 3A) intrudes both the pinkish granite (Fig. 6A) and the associated mafic-intermediate rocks (Fig. 4A). Mafic-intermediate bodies at the eastern margin of the Santa Eulália-Monforte massif are intruded by the pinkish granite (Figs. 3B and 6C, D, E). Angular mafic enclaves (Fig. 5B) seem to represent early cooled pieces of gabbro caught up in the granodiorite-quartzdiorite-tonalite magma, but the variation from sharp though irregular contacts to more diffuse contacts suggests that they are contemporaneous (Fig. 4E). It is notable the presence of composite enclaves (Fig. 3E) and irregular patches of granodiorite-quartzdiorite-tonalite (Fig. 3D) hosted by gabbro-diorite, together with a channel-like enclave swarm of mafic-intermediate rocks (Fig. 4C; D) suggest intermingling of two magmas. Gabbro-dioritic rocks include leucocratic veins and lenses of quartzdiorite and/or tonalite (Fig. 3C; D). The occurrence of K-feldspar within the gabbro-dioritic enclaves, which may be the same as that of the host granitic rock (Fig. 5), suggests that granitic magma could have interacted with the mafic-intermediate magmas, probably at a time when both were not completely crystallized. The existence of mafic-intermediate enclaves with irregular, rounded and elliptical shapes, suggests mingling with the host granitic magma (Fig. 5).

U-PB GEOCHRONOLOGY

Sample preparation and analytical methods

Zircon separation from a sample of granite (MFT-1) and a sample of gabbro-diorite (BCA-2) of the external ring of the Santa Eulália-Monforte massif (sampling sites on Fig. 2) was performed by means of traditional techniques using dense liquids and magnetic separation at the University of Évora (Portugal). Selected crystals were hand-picked using a binocular lens. Zircon concentrates were cast on a 3.5cm diameter epoxy mount, together with zircon standards (TEMORA zircon, SL13 zircon and GAL zircon), then polished and documented using SEM-CL (Fig. 8), at the IBERSIMS (University of Granada, Spain). Mounts were coated with gold (80-microns thick) and inserted into the SHRIMP for analysis.

Each selected spot was rastered with the primary beam during 120s prior to analysis, and then analyzed over 6 scans following the isotope peak sequence $^{196}Zr_2O$, ^{204}Pb, 204.1 background, ^{206}Pb, ^{207}Pb, ^{208}Pb, ^{238}U, ^{248}ThO, ^{254}UO. Every peak of each scan was measured sequentially 10 times with the following total counts per scan: 2s for mass 196; 5s for masses 238, 248, and 254; 15s for masses 204, 206, and 208; and 20s for mass 207. The primary beam, composed of $^{16}O^{16}O^{2+}$, was set to an intensity of 4 to 5nA, using a 120-micron Kohler aperture, which generates 17 x 20micron elliptical spots on the target. The secondary beam exit slit was set at 80microns, achieving a resolution of about 5,000 at 1% peak height. All calibration procedures were performed

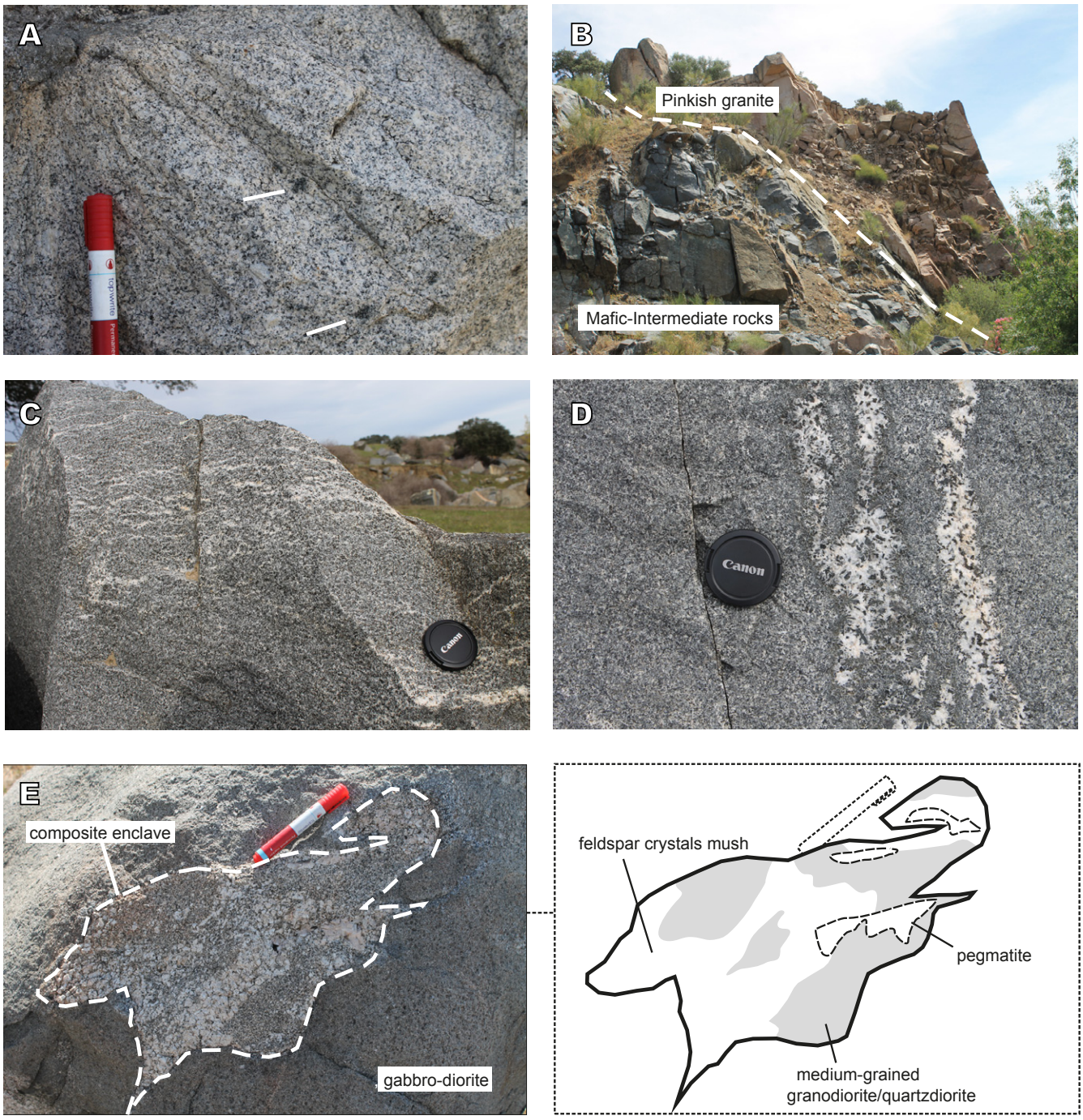

FIGURE 3. Representative field relationships of the main rock types of the Santa Eulália-Monforte massif: A) greyish granite from the core, containing megacrystals of cordierite; B) sharp contact between the coarse-grained pinkish granite and the mafic-intermediate rocks from the external ring, C) intermediate (dioritic) and D) mafic (gabbroic) bodies from the external ring, with leucocratic veins; E) composite enclave with irregular shape consisting of medium-grained quartzdiorite/granodiorite, coarse-grained K- feldspar mush and pegmatite, surrounded by gabbro-dioritic rocks.

on the standards included on the same mount. Mass calibration was performed on the GAL zircon (*ca.* 480Ma, very high U, Th and common lead content; Montero *et al.*, 2008). Analytical sessions initially involved the measurement of SL13 zircon (Claoué-Long *et al.*, 1995), which was used as a concentration standard (238ppm U). TEMORA zircon (*ca.* 417Ma, Black *et al.*, 2003), used as isotope ratios standard, was then measured every four unknowns.

Data reduction was performed using the SHRIMPTOOLS software specifically developed

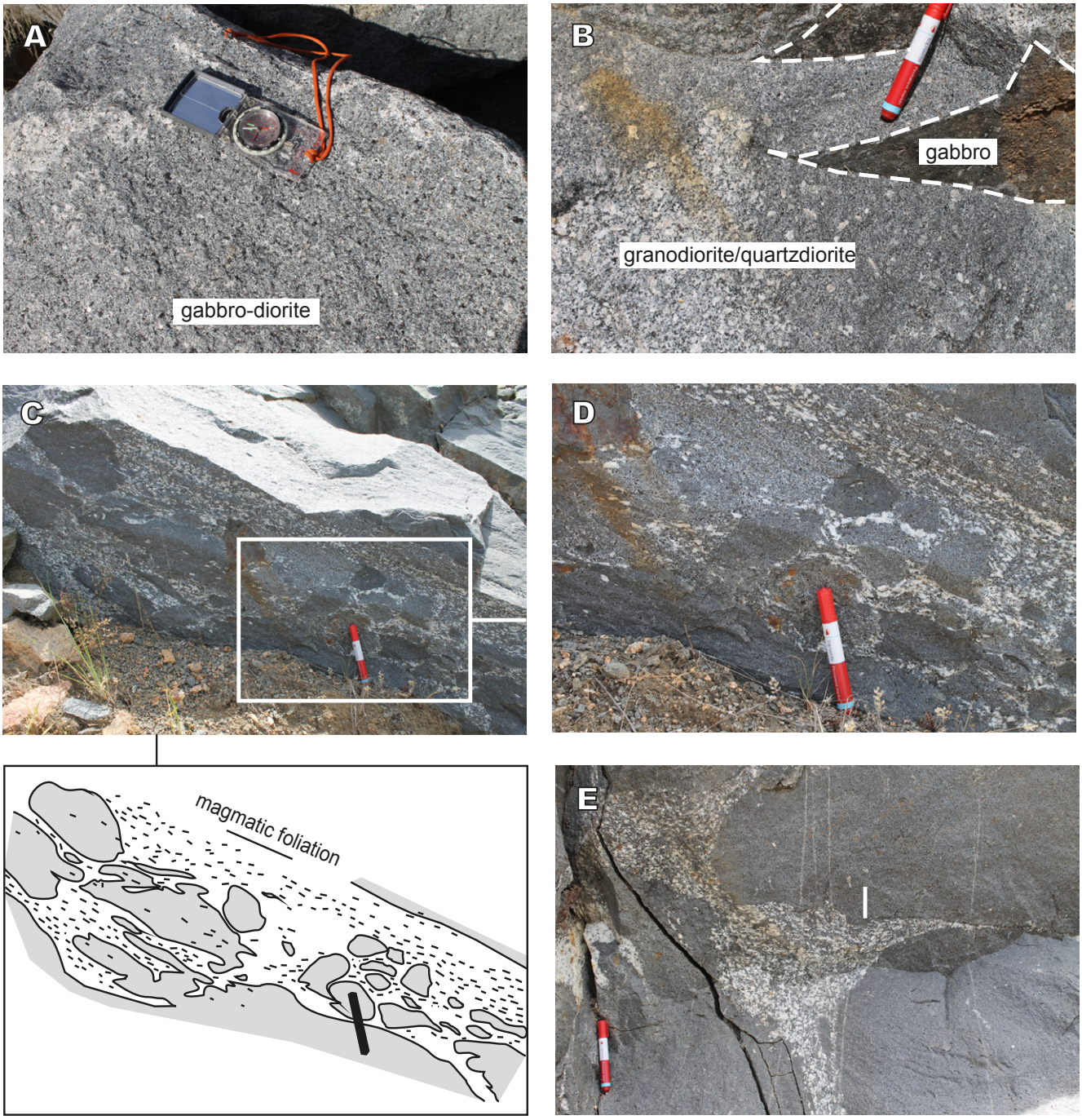

FIGURE 4. Representative field relationships of the mafic-intermediate rocks of the Santa Eulália-Monforte massif: A) gabbro-diorite; B) cuspate-shape contact between the quartzdiorite-granodiorite and the surrounded gabbro-diorite containing K-feldspar crystals, apparently similar to those of the quartzdiorite-granodiorite; C) channel-like enclave swarm of mafic-intermediate rocks with magmatic foliation defined by the preferred orientation of K-feldspar crystals; D) detail of C) showing various enclave rock types (gabbro, gabbro-diorite and quartzdiorite/granodiorite) and sizes enclosed in quartzdiorite/granodiorite and felsic aggregates, mainly formed of large K-feldspar crystals; E) flame structures filled by quartzdiorite/granodiorite with large K-feldspar crystals.

for IBERSIMS (available at www.ugr.es/~fbea). The intensity of each measured isotope was calculated in two steps using the software: first, the STATA letter-value display algorithm was used to find outliers in the ten replicates measured at each peak during each scan, discarding them and averaging the rest once they had been normalized to SBM measurements; then, for each isotope, a robust regression of each scan average *versus*

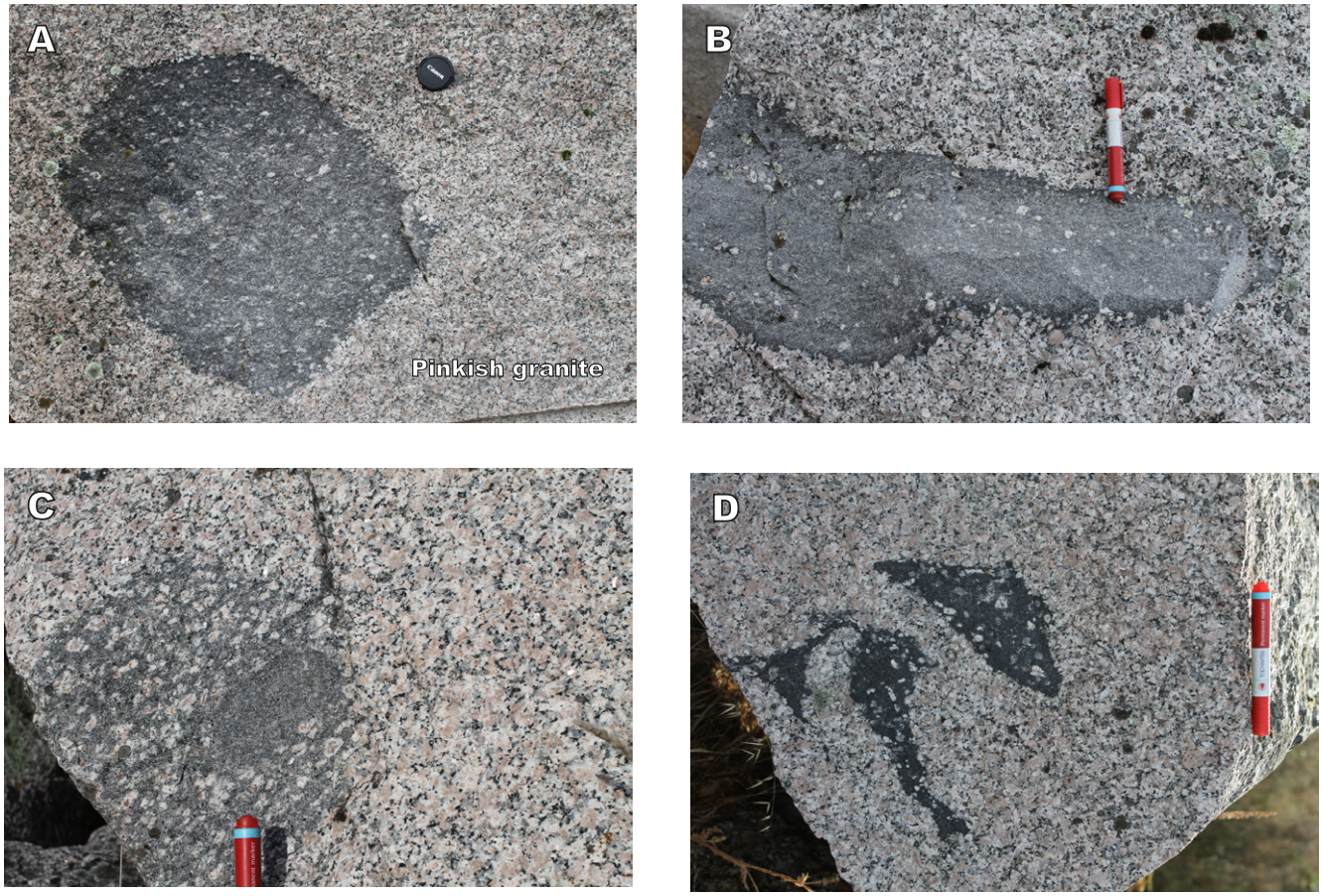

FIGURE 5. Mesoscale details of host-enclave relationships in the coarse-grained pinkish granite from the external ring of the Santa Eulália-Monforte massif: A) rounded enclave of mafic-intermediate rock with crenulated contact; B) elongated enclave of intermediate rock with a biotite-rich rim, derived from the enclave-host reaction, along the irregular contact, and K-feldspar phenocrysts aligned to the major axis of the enclave; C) composite intermediate enclave; D) curved and irregular shape mafic enclaves. All mafic and intermediate enclaves of this figure contain K-feldspar phenocrysts similar to those of the host granite.

time, if measured, was performed. The final result for each isotope was calculated as the value at the mid-time of the analysis resulting from a robust regression line. Errors (95% confidence level) were calculated as the standard error of the linear prediction at the mid-point of the analysis. $^{206}Pb/^{238}U$ was calculated from the measured $^{206}Pb^{+}/^{238}U^{+}$ and UO^{+}/U^{+} following the method described by Williams (1998). For high-U zircons (U>2,500ppm) $^{206}Pb/^{238}U$ was further corrected using the algorithm of Williams and Hergt (2000). Plotted and tabulated analytical uncertainties are 1σ precision estimates. Uncertainties in calculated mean ages are 95% confidence limits (tσ, where t is the Student's t multiplier) and, for mean $^{206}Pb/^{238}U$ ages, include the uncertainty in Pb/U calibration (0.3-0.5%). Common Pb corrections assumed a model common Pb composition appropriate to the age of each spot (Cumming and Richards, 1975). U-Th-Pb data are presented in Table 1 (electronic appendix, available at www.geologica-acta.com) and plotted in Figure 9, using Isoplot 4 (Ludwig, 2009).

RESULTS

Sample MFT-1 (granite)

Most zircons are stubby and elongated euhedral prisms (150-300μm diameter in the long-axis) (Fig. 8). Morphologically complex zircons analyzed show cores of variable size (dark-cathodoluminescence (CL) subeuhedral cores with concentric zoning and wavy extinction, sub-euhedral cores of a patchy to irregular texture with linear or wavy dark and bright-CL bands, sub-rounded dark-CL and unzoned cores). Cores are surrounded by concentric zoned to unzoned rims (Fig. 8). Few grains are simple, showing banded or concentric zoning and some show discordant zircon overgrowths or recrystallization textures. Twenty-nine U-Th-Pb isotopic analyses of 25 representative zircon grains are listed in Table 1. Twenty-five $^{206}Pb/^{238}U$ ages in the range *ca.* 536 to 273Ma, were obtained using 204-lead correction and show a discordance ≤5%. The oldest age of *ca.* 537Ma (Cambrian), obtained in analysis

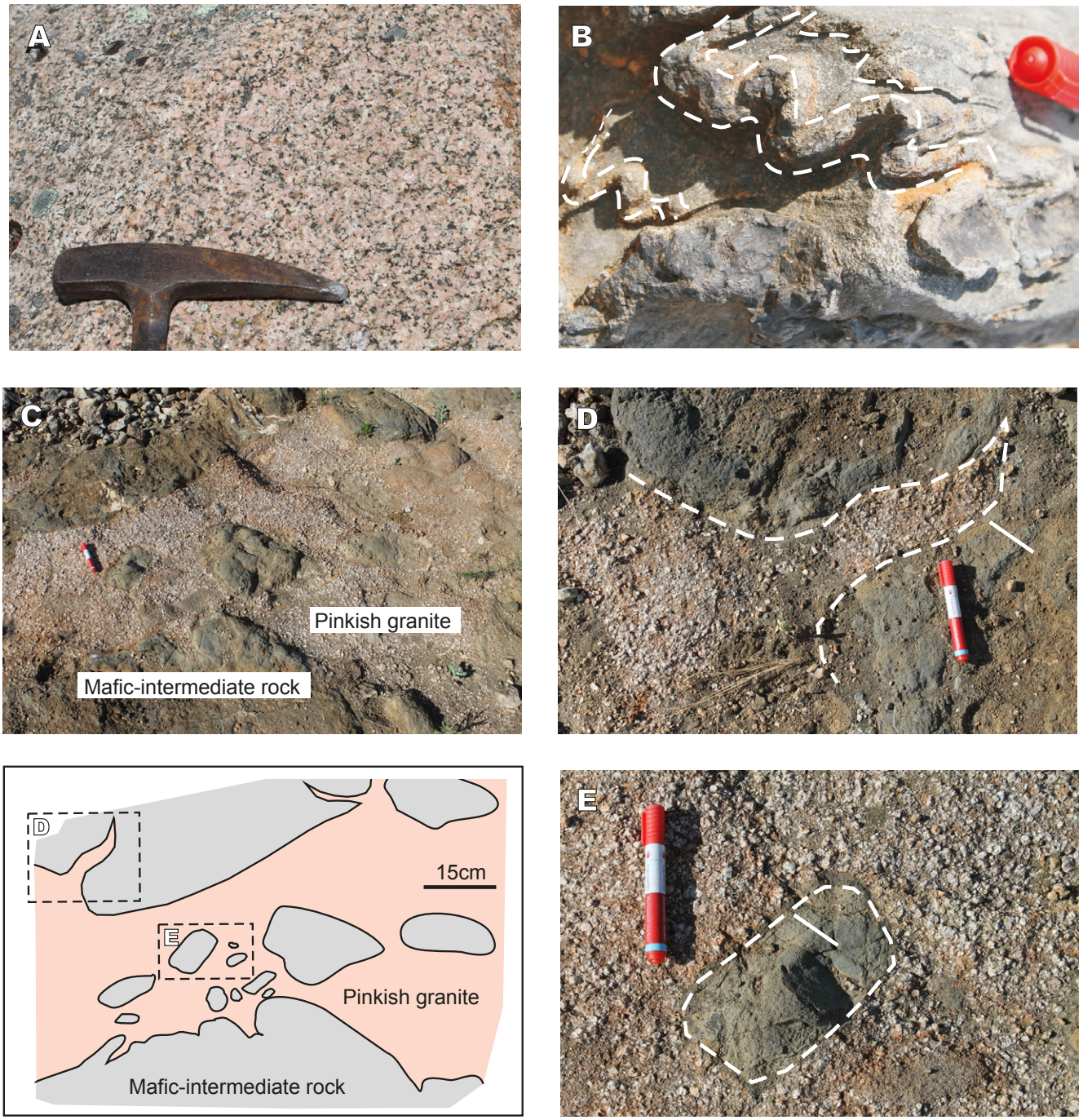

FIGURE 6. Representative field relationships between the pinkish granite and the mafic-intermediate rocks of the Santa Eulália-Monforte massif and surrounding country rocks: A) coarse-grained pinkish granite from a dyke cutting across mafic-intermediate rocks; B) xenolith of a previously folded and metamorphosed carbonate rock from the Coimbra-Córdoba shear zone; C) mafic-intermediate rocks intruded by the pinkish granite; D) apophysis of granite; E) mafic enclave with a fine-grained and biotite-rich reaction rim.

8.2, is interpreted as an inherited old core and, indeed, close inspection showed that it is surrounded by a young overgrowth (8.1). The remaining 19 $^{206}Pb/^{238}U$ ages were obtained in zircons with a wide range of U (295-2,277ppm) and Th (118-1,763ppm) contents, and an average Th/U ratio of 0.37 (error standard deviation=0.03; Fig. 9A). These 19 U-Th-Pb isotopic compositions yielded a weighted mean $^{206}Pb/^{238}U$ age of 296±4Ma (MSWD=0.62). However, the omission of three analyses with high-U (10.1, 14.1 and 16.1) gave a weighted mean $^{206}Pb/^{238}U$ age of 297±4Ma (MSWD=0.43; Fig. 9B), which is probably the best estimate of the crystallization age of the granite.

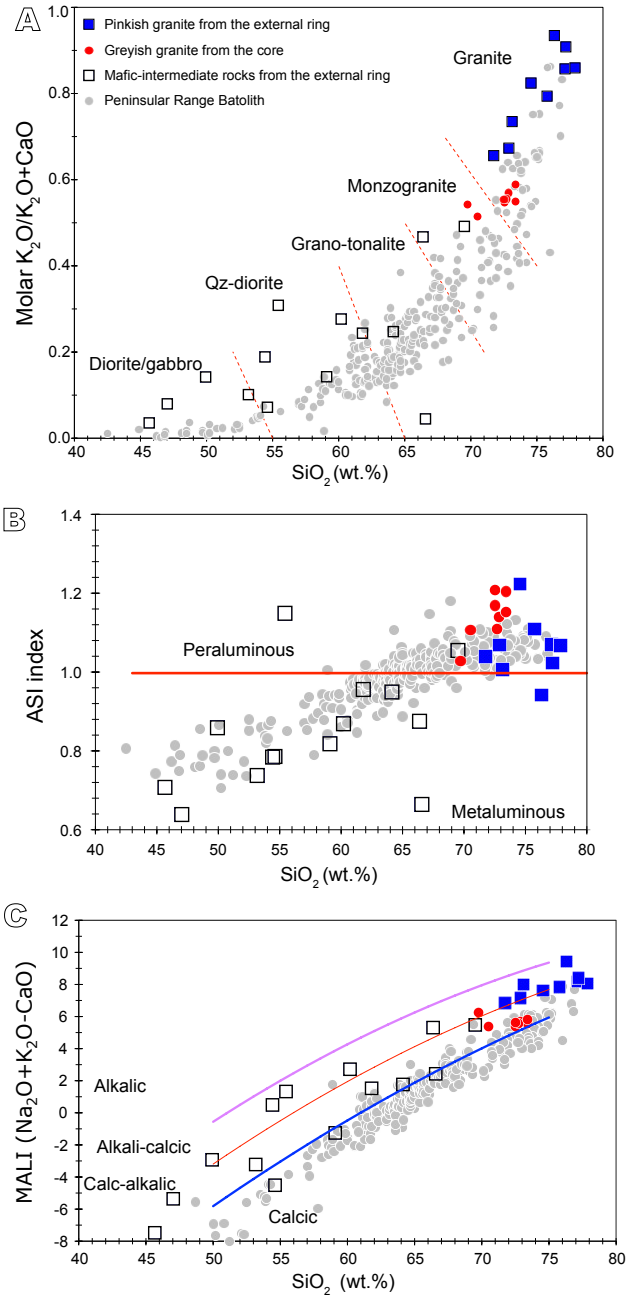

FIGURE 7. Geochemical diagrams showing essential variations of representative plutonic rocks of the Santa Eulália-Monforte massif. The geochemical data of the Santa Eulália-Monforte massif presented in these diagrams were compiled from Carrilho Lopes *et al.* (1998) and González Menéndez *et al.* (2006). The Peninsular Range batholith, representing Mesozoic continental arcs formed on the edge of the Precambrian North American craton by subduction of the Farallon oceanic Plate beneath North America, is used as comparative data (grey dots), taken as representative of the calc-alkaline trend (Lee *et al.*, 2007). A) SiO_2 *vs.* K_2O/K_2O+CaO diagram shows the compositional range of the mafic-intermediate plutonic rocks and the position of the greyish granite from the core between the pinkish granite and the mafic-intermediate rocks forming the external ring. B) SiO_2 *vs.* ASI index diagram indicating the peraluminous character of almost all granites of the Santa Eulália-Monforte massif. C) The relation between the SiO_2 content and the MALI index (Frost *et al.*, 2001) delimits the trend of Santa Eulália-Monforte massif as calc-alkalic and alkali-calcic, above the typical calc-alkaline trend.

Sample BCA-2 (gabbro-diorite)

Zircons of this sample present morphological differences with respect to those of the granite described above. CL images of stubby and elongated euhedral prisms (150-350μm diameter in long-axis) show simpler internal textures. Most zircon grains have banded zoning (Fig. 8), but a few show oscillatory concentric zoning or are unzoned.

Twenty-four U-Th-Pb isotopic analyses of representative zircon grains are listed in Table 1. Common lead 204-lead corrected isotope ratios gave $^{206}Pb/^{238}U$ ages of *ca.* 319-248Ma, having a cluster between *ca.* 310Ma and 290Ma. Sixteen U-Th-Pb analyses with discordance of ≤5% were performed on zircons characterized by a wide range of U (89-629ppm) and Th (54-343ppm) content and average Th/U ratio of 0.64 (error standard deviation=0.02; Fig. 9A). This group of analyses yielded a concordia age of 303±3Ma (MSWD=0.079; Fig. 9D) overlapping the weighted mean $^{206}Pb/^{238}U$ age of 303±4Ma (MSWD=1.01; Fig. 9E), which is probably the best estimate for the crystallization age of the gabbro-diorite.

DISCUSSION

Significance of the obtained U-Th-Pb data

The new obtained U-Pb ages of the Santa Eulália-Monforte massif suggest that the gabbro-diorite (*ca.* 303Ma) crystallized somewhat 6Ma earlier than the external granite (*ca.* 297Ma) (Figs. 9 and 10). However, the overlapping ages of zircons shown in Figure 10 suggest that the mafic-intermediate rocks and the pinkish granite can also be roughly contemporaneous, as documented by field data. In some cases, it has been demonstrated that zircon populations in a magma chamber are a mix of autocrysts, antecrysts, and xenocrysts, and that the resultant plutonic rocks are, thus, a mechanical mixture of crystals (*e.g.* Charlier *et al.*, 2005; Miller *et al.*, 2007) that may have different individual ages. The obtained data suggest that the external ring of the Santa Eulália-Monforte massif formed by the crystallization of injections of compositionally distinct magmas. These magmas were close enough in time so that the earlier gabbro-dioritic magma had not cooled yet and had differentiated significantly before the addition of the later granitic magma.

The Th/U ratios obtained from analyzed zircons of both samples (Fig. 10) prove the coexistence of two compositionally distinct magmas from which zircon crystallized during the evolutionary history of the bimodal magmatic chamber. The average Th/U ratio of the granite (0.40) is significantly lower than that of the gabbro-diorite (0.64), indicating felsic-intermediate

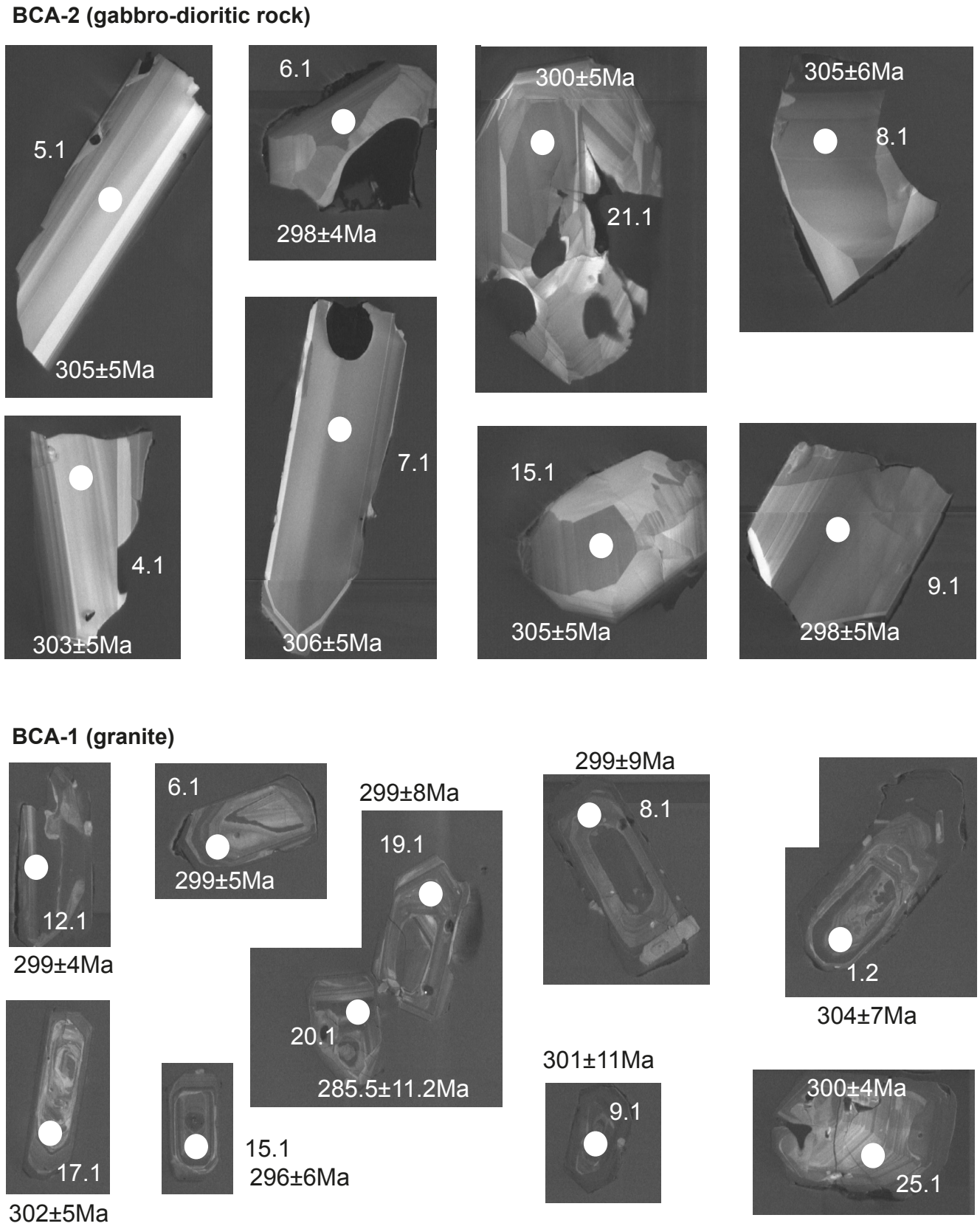

FIGURE 8. Cathodoluminiscence (CL) imaging of representative zircons of the samples BCA-2- gabbro-dioritic rock and MFT-1- pinkish granite, with analytical sites and their resulting $^{206}Pb/^{238}U$ ages indicated. Analysis spots and ages are listed in Table I.

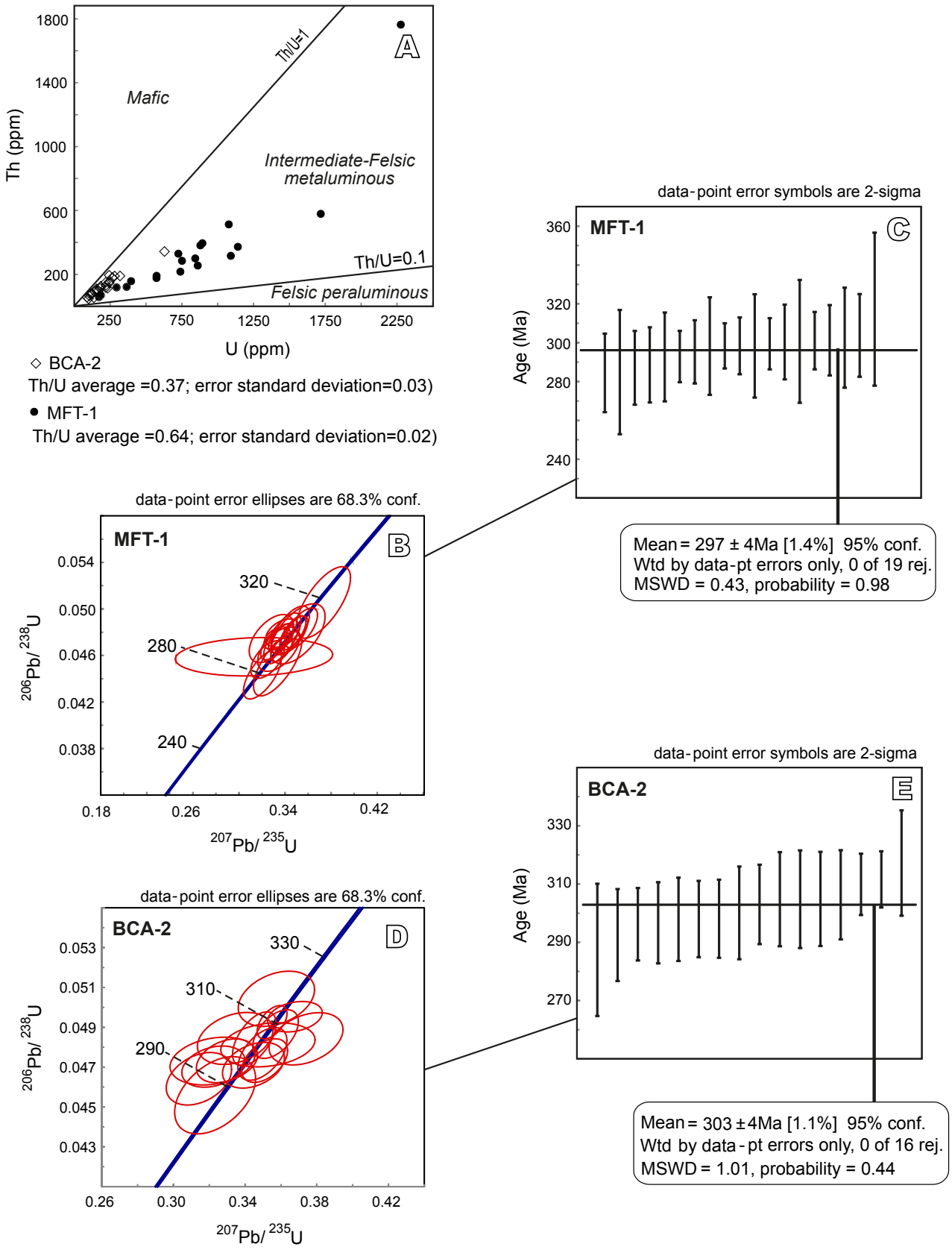

FIGURE 9. U-Th-Pb data: A) Th *vs.* U diagram with the fields that reflect different sources composition of melt from which zircon crystallized; B) and C) weighted mean and Concordia diagram of $^{206}Pb/^{238}U$ ages for sample MFT-1, respectively; D) and E) Concordia diagram and weighted mean of $^{206}Pb/^{238}U$ ages for sample BCA-2, respectively.

metaluminous sources for the two magmas (Heaman *et al.*, 1990; Hanchar and Miller, 1993, Hoskin and Schaltegger, 2003). In Figure 6, most zircon analyses of granite (sample MFT-1) are plotted in the range of 0.3<Th/U ratio<0.5, closer to the field of felsic peraluminous sources, in which probably there is abundant monazite (Th>U), and lower than those from the gabbro-diorite (sample BCA-2), in the range of 0.5<Th/U ratio<0.7, in which there is no other U-Th accessory.

Age relationship of the Santa Eulália-Monforte massif with other LC-EP Iberian calc-alkaline plutonic rocks

The reported weighted mean $^{206}Pb/^{238}U$ ages (this study) for the plutonic rocks of the external ring of the Santa Eulália-Monforte massif is of 303±3Ma (Late Carboniferous) for the gabbro-diorite and of 297±4Ma (Early Permian) for the granite. T-test indicates that the difference between these two zircon age populations is statistically significant (p-value is 0.02, *i.e.* lower than 0.05). Field observations of the consistent intrusive relationships between the greyish granite and the external ring (Gonçalves and Coelho, 1969-1970; Gonçalves, 1971; Oliveira, 1975; Gonçalves *et al.*, 1972, 1975; Carrillho Lopes *et al.*, 1998; González Ménendez *et al.*, 2006; Sant'Ovaia *et al.*, 2015) also suggest that these intrusions are coeval. Crystallization ages of the calc-alkaline magmatic rocks of the Santa Eulália-Monforte massif are within the wider range of ages obtained for other post-kinematic magmatic rocks of the Iberian Massif: i) the neighboring calc-alkaline Nisa-Alpalhão and Los Pedroches batholiths (U-Pb zircon ages of *ca.* 314-304Ma; Carracedo *et al.*, 2008; Solá *et al.*, 2009) (Fig. 1); ii) the calc-alkaline plutonic rocks of the Central Iberian and West-Asturian Leonese zones (U-Pb zircon ages of *ca.* 312-286Ma; Valverde-Vaquero, 1997; Dias *et al.*, 1998; Montero *et al.*, 2004; Valle Aguado *et al.*, 2005; Bea *et al.*, 2006; Neiva *et al.*, 2009; Fernández-Suárez *et al.*, 2011; Gutiérrez-Alonso *et al.*, 2011; Valverde-Vaquero *et al.*, 2011; Díaz Alvarado *et al.*, 2013; Díez Fernández and Pereira, 2017); and iii) the volcanic and plutonic rocks of the Central-eastern Pyrenees (U-Pb zircon ages of *ca.* 314-283Ma; Roberts *et al.* 2000; Aguilar *et al.*, 2014; Druguet *et al.*, 2014; Pereira *et al.*, 2014; and $^{40}Ar/^{39}Ar$ ages in the range of *ca.* 291-285Ma; Solé *et al.*, 2002). Our new U-Pb ages are *ca.* 20Ma younger with regard to the published age estimates for the Variscan plutonism and high-medium grade metamorphism recorded in the Ossa-Morena Zone (*ca.* 353-324Ma; Fig. 1). This age relationship indicates that the undeformed calc-alkaline magmatic rocks of the Santa Eulália-Monforte massif are consistent with a post-Variscan intrusion (*i.e.* post-kinematic), representing so far the youngest LC-EP calc-alkaline magmatic event of the Ossa-Morena Zone. The emplacement of the Santa Eulália-Monforte massif immediately followed the neighboring calc-alkaline granite intrusion of the Nisa-Albuquerque massif (*ca.* 309-306Ma; Solá *et al.*, 2009) and, in part, was almost synchronous to the latest magmatic pulses of the Los Pedroches massif (*ca.* 309-304Ma; Carracedo *et al.*, 2008) (Fig. 1).

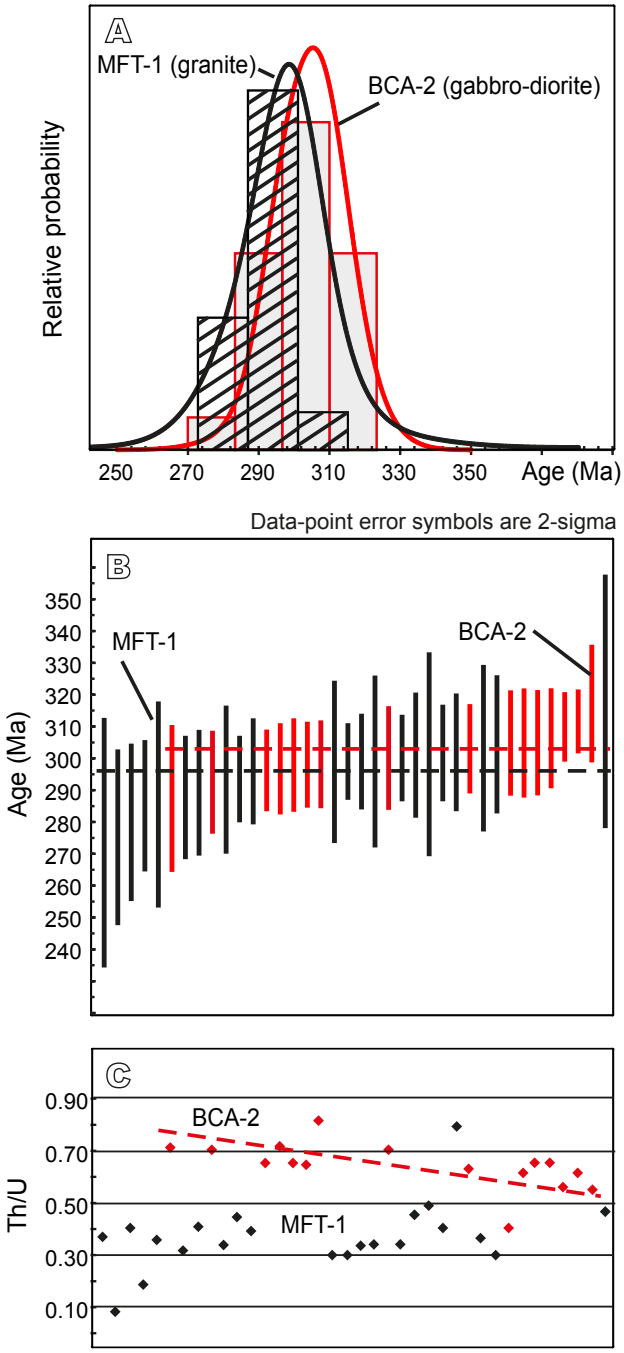

FIGURE 10. Joint projection of samples BCA-2 and MFT-1 U-Pb results: A) Age and probability density diagrams, B) weighted mean of $^{206}Pb/^{238}U$ ages, and C) Th/U ratio *vs.* age diagram.

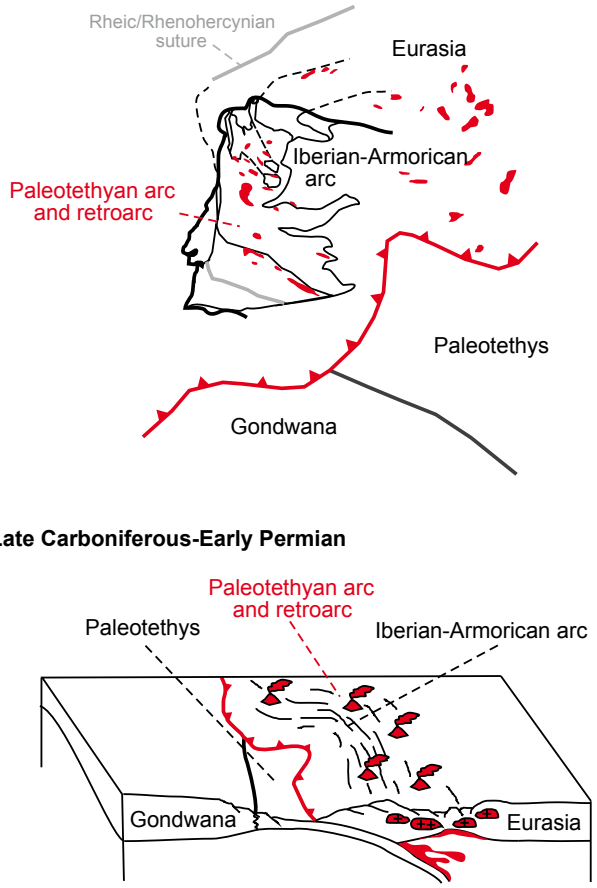

FIGURE 11. Schematic diagrams with the reconstruction of: A) the Iberian-Armorican arc and Paleotethyan arc and forearc at Early Carboniferous, after the closing of the Rheic (or Rheno-Hercynian) Ocean, and before the end of the subduction at the western corner of the Paleotethys Ocean; B) the oceanic-continental subduction zone and the formation of plumes resulting from the dehydration of the subducted crust, aqueous fluid transport, partial melting, melt extraction, and melt emplacement in the form of volcanism and intrusive plutons likewise, at the Santa Eulália-Monforte massif (modified from Pereira *et al.*, 2015b and references therein).

Geodynamic model

There is a general acceptance of a single, consensual interpretation that supports the growth of the Iberian LC-EP batholiths within the framework of the Variscan orogenic cycle ("late-Variscan batholiths"). This interpretation is considered valid even if the origin of these calc-alkaline magmas is about 60-80Ma younger than the development of the Rheic Ocean active margin (Martínez Catalán *et al.*, 2009; Díez Fernández *et al.*, 2016; Pereira *et al.*, 2017b). This paradigm disregards the wider context of the amalgamation of the Pangaea and the spatial proximity of Iberia relative to the Eurasian active margin during the LC-EP closing of the Paleotethys Ocean (Pereira *et al.*, 2015b).

The generation of LC-EP post-kinematic I-type calc-alkaline Iberian batholiths in a tectonic setting other than subduction conflicts with essential thermal requirements and phase equilibria constraints on metaluminous magma generation and fractionation (Pereira *et al.*, 2015b). The emplacement and thermal effects of the LC-EP calc-alkaline batholiths into a fertile middle crustal level, dominated by several kilometer-thick fertile Ediacaran-Cambrian metasedimentary successions, explains the late generation of S-type peraluminous granitic rocks and local hybridization of the intrusive magma, which became more peraluminous and potassic (Díaz Alvarado *et al.*, 2011; 2013). The lower crust is usually mentioned as the source of the Iberian calc-alkaline batholiths based on the assumptions that they are intrusive into the middle crust and that melts produced from the mantle underlying the continental crust must be basaltic (Dias *et al.*, 1998; Neiva *et al.*, 2009, 2012; Villaseca *et al.*, 2009, 2012). The new conception of subduction-related magmatism ownig to plume-assisted relamination (Gerya *et al.*, 2004; Castro *et al.*, 2010; Gerya and Meilick, 2011; Vogt *et al.*, 2012) assumes that the generation of magmas of intermediate composition (andesite-diorite) occurs by means of the melting of subducted materials in silicic composite plumes, *i.e.* composed of oceanic crust and sediments. These materials are later relaminated to a level below the lower crust, where they split by melt segregation into liquids that are emplaced in the middle and upper crust (batholiths) and residues that remain in the lower crust as mafic granulites (Castro, 2013, 2014). In the case of the LC-EP calc-alkaline Iberian magmatism, several factors indicate an extra-crustal origin (Castro *et al.*, 2010, 2013; Castro, 2013, 2014; Pereira *et al.*, 2015b). The LC-EP Iberian batholiths have close compositional similarities with the calc-alkaline silicic magmatism of active continental margins as the Andes (Patagonian batholith) and the North American Cordillera (Sierra Nevada batholith). They also include arc-related appinitic rocks, suggesting a link to a subduction setting (Murphy, 2013) similar to that of the post-Paleozoic Cordilleran batholiths formed at the Pacific active margin of the Americas (Castro *et al.*, 2011). The period during which LC-EP calc-alkaline magmatism was generated (*ca.* 315-280Ma) coincides with the development of the Iberian-Armorican Arc (Fig. 11) (*i.e.* Cantabrian orocline; Gutiérrez-Alonso *et al.*, 2008, 2011; Fernández-Suárez *et al.*, 2011; Weil *et al.*, 2012; Johnston *et al.*, 2013), which was probably related to the Pangaea self-subduction (Gutiérrez-Alonso *et al.*, 2008, 2011). In a global context, during the Late Carboniferous the western zones of the Iberian Massif were affected by the late stages of the Laurussia-Gondwana convergence, whereas the subduction of the Paleotethyan Ocean prevailed during and after LC-EP times (Cimmerian cycle) along the Eurasian eastern domains (Stampfli and Borel, 2002; Stampfli *et al.*, 2013) (Fig. 11). The progression of the Paleotethys subduction led to the collision between Cimmerian terranes (detached from the non-collisional northern margin of

Gondwana) and the Eurasian active margin (Cocks and Torsvik, 2006; Stampfli and Kozur, 2006), which can explain the inception of a LC-EP Paleotethyan magmatic arc in Iberia (Fig. 11; Pereira *et al*., 2015b).

CONCLUSIONS

This paper presents the first SHRIMP U-Pb zircon dating of the Santa Eulália-Monforte massif. Concordia and weighted average zircon ages from granite and gabbro-diorite samples indicate magmatic crystallization at *ca*. 297Ma and 303Ma, respectively. However, field evidence and full analysis of zircon ages do not definitively rule out that they may have been contemporaneous during a certain stage of magma emplacement.

The Santa Eulália-Monforte massif represents so far the youngest LC-EP calc-alkaline magmatic event of the Ossa-Morena Zone (*ca*. 303-297Ma), which immediately followed the neighboring calc-alkaline granite production of the Nisa-Albuquerque massif (*ca*. 309-306Ma) and in part, was almost synchronous to the latest magmatic pulses of the Los Pedroches massif (*ca*. 309-304Ma). The LC-EP Iberian magmatism was coeval with the formation of the Iberian-Armorican arc (Cantabrian orocline). The LC-EP Iberian magmatism can be framed into a plausible model of a transient continental magmatic arc developed in the Eurasian convergent Plate margin above the subducted Paleotethys oceanic Plate.

ACKNOWLEDGMENTS

Financial support has been provided by Fundação para a Ciência e Tecnologia (Portugal) through research projects "GOLD" (PTDC/GEO-GEO/2446/2012: COMPETE: FCOMP-01-0124-FEDER-029192) and "LITHOS" (CGL2013-48408-C3-1-P). C. Rodríguez appreciates the financial support from Universidad de Huelva (Spain) through its postdoctoral program (under the "Estrategia Politíca Científica de la UHU 2016/2017 in collaboration with the Universidade de Évora (Portugal)). This is the IBERSIMS publication Nº 44. The authors are grateful for the critical spirit of the comments made by the editors of this volume, by J.B. Silva, R. Díez Fernández and an anonymous reviewer, who helped to greatly improve this work.

REFERENCES

Aguilar, C., Liesa, M., Castiñeiras, P., Navidad, M., 2014. Late Variscan metamorphic and magmatic evolution in the eastern Pyrenees revealed by U-Pb age zircon dating. Journal of the Geological Society, London, 171(2), 181-192.

Alcock, J.E., Martínez Catalán, J.R., Rubio Pascual, F.J., Montes, A.D., Díez Fernández, R., Gómez Barreiro, J., Arenas, R., Dias da Silva, Í., González Clavijo, E., 2015. 2-D thermal modeling of HT-LP metamorphism in NW and Central Iberia: Implications for Variscan magmatism, rheology of the lithosphere and orogenic evolution. Tectonophysics, 657, 21-37.

Apalategui, O., Eguiluz, L., Quesada, C., 1990. Ossa-Morena zone: Structure. In: Dallmeyer, R.D., Martínez García, E., (eds.). Pre-Mesozoic Geology of Iberia. Berlin, Germany, Springer-Verlag, 280-292.

Barbarin, B., 2005. Mafic magmatic enclaves and mafic rocks associated with some granitoids of the central Sierra Nevada batholith, California: nature, origin, and relations with the hosts. Lithos, 80, 155-177.

Bea, F., 2004. La naturaleza del magmatismo de la Zona Centro Ibérica: consideraciones generales y ensayo de correlación. In: Vera, J.A. (ed.). Geología de España. Ed. Sociedad Geológica de España (SGE) - Instituto Geológico y Minero de España (IGME), Madrid, 128-133.

Bea, F., Montero, P., Molina, J.F., 1999. Mafic precursors, Peraluminous Granitoids, and Late Lamprophyres in the Avila Batholith: A Model for the Generation of Variscan Batholiths in Iberia. Journal of Geology, 107, 399-419.

Bea, F., Montero, P., Zinger, T., 2003. The nature, origin, and thermal influence of the granite source layer of Central Iberia. Journal of Geology, 111, 579-595.

Bea, F., Montero, P., González Lodeiro, F., Talavera, C., Molina, J.F., Scarrow, J.H., Whitehouse, M.J., Zinger, T., 2006. Zircon thermometry and U-Pb ion-microprobe dating of the gabbros and associated migmatites of the Variscan Toledo Anatectic Complex, Central Iberia. Journal of the Geological Society, 163, 847-855.

Black, L.P., Kamo, S.L., Williams, I.S., Mundil, R., Davis, D.W., Korsch, R.J., Foudoulis, C., 2003. The application of SHRIMP to Phanerozoic geochronology, a critical appraisal of four zircon standards. Chemical Geology, 200, 171-188. DOI:10.1016/S0009-2541 (03) 00166-9.

Burg, J., Iglesias, M., Laurent, P., Ribeiro, A., 1981. Variscan intracontinental deformation: The Coimbra-Córdoba shear zone (SW Iberian Peninsula). Tectonophysics, 78, 161-177.

Cambeses, A., Scarrow, J.H., Montero, P., Molina, J.F., Moreno, J.A., 2015. SHRIMP U-Pb zircon dating of the Valencia del Ventoso plutonic complex, Ossa-Morena Zone, SW Iberia: Early Carboniferous intra-orogenic extension related 'calc-alkaline' magmatism. Gondwana Research, 8, 735-756. DOI:10.1016/j.gr.2014.05.013

Carracedo, M., Paquette, J.L., Alonso Olazabal, A., Santos Zalduegui, J.F., García de Madinabeitia, S., Tiepolo, M., Gil Ibarguchi, J.I., 2008. U-Pb dating of granodiorite and granite units of the Los Pedroches batholith. Implications for geodynamic models of the southern Central Iberian Zone (Iberian Massif). International Journal of Earth Sciences (Geologishe Rundschaw), 98: 1659. DOI: 10.1007/s00531-008-0317-0.

Carrilho Lopes, C.J.M., Munha, J.M., Wu, C.T., Oliveira, V.M.J., 1998. O complexo plutónico de Monforte-Santa Eulália (Alentejo-NE, Portugal Central): caracterização geoquímica e considerações petrogenéticas. [In Portuguese] Comunicações do Instituto Geológico e Mineiro, 83, 127-142.

Castro, A., 2013. Tonalite-granodiorite suites as cotectic systems: A review of experimental studies with applications to granitoid petrogenesis. Earth Science Reviews, 124, 68-95.

Castro, A., 2014. The off-crust origin of granite batholiths. Geoscience Frontiers, 5, 63-75.

Castro A., Patiño Douce, A.E., Corretgé, L.G., de la Rosa, J.D., El-Biad, M., El-Hmidi, H., 1999. Origin of peraluminous granites and granodiorites, Iberian Massif, Spain: an experimental test of granite petrogenesis. Contributions to Mineralogy and Petrology, 135, 255-276.

Castro, A., Corretgé, L.G., de la Rosa, J., Enrique, P., Martínez, F.J., Pascual, E., Lago, M., Arranz, E., Galé, C., Fernández, C., Donaire, T., López, S., 2002. Paleozoic magmatism.In: Gibbons, W., Moreno, M. T. (eds.). The Geology of Spain. London. Geological Society, 649pp.

Castro, A., Corretgé, L.G., de la Rosa, J.D., Fernández, C., López, S., Chacón, H., 2003. The appinite–migmatite complex of Sanabria, NW Iberian massif, Spain. Journal of Petrology, 44, 1309-1334.

Castro, A., Gerya, T., García-Casco, A., Fernández, C., Díaz Alvarado, J., Moreno-Ventas, I., Loew, I., 2010. Melting relations of MORB-sediment mélanges in underplated mantle wedge plumes. Implications for the origin of cordilleran-type batholiths. Journal of Petrology, 51, 1267-1295.

Castro, A., Moreno-Ventas, I., Fernández, C., Vujovich, G., Gallastegui, G., Heredia, N., Martino, R.D., Becchio, R., Corretgé, L.G., Díaz-Alvarado, J., García-Arias, M., Liu, D.-Y., 2011. Petrology and SHRIMP U-Pb zircon geochronology of Cordilleran granitoids of the Bariloche area, Argentina. Journal of South American Earth Sciences, 32, 508-530.

Castro, A., Vogt, K., Gerya, T.V., 2013. Generation of new continental crust by sublithospheric silicic-magma relamination in arcs: A test of Taylor's andesite model. Gondwana Research, 23, 68-95.

Charlier, B.L.A., Wilson, C.J.N., Lowenstern, J.B., Blake, S., Van Calsteren, P.W., Davidson, J.P., 2005. Magma generation at a large, hyperactive silicic volcano (Taupo, New Zealand) revealed by U-Th and U-Pb systematics in zircons. Journal of Petrology, 46, 3-32.

Claoué-Long, J.C., Compston, W., Roberts, J., Fanning, C.M., 1995. Two Carboniferous ages: a comparison of SHRIMP zircon dating with conventional zircon ages and $^{40}Ar/^{39}Ar$ analysis. In: Berggren, W. A., Kent, D. V., Aubry, M. P., Hardenbol, J., (eds.). Geochronology Time Scales and Global Stratigraphic Correlation. Society for Sedimentary Geology (SEPM), Special Publication No. 4, 3-21.

Cocks, L.R.M., Torsvik, T.H., 2006. European geography in a global context from the Vendian to the end of the Palaeozoic. In: Gee, D.G., Stephenson, R.A., (eds.). European Lithosphere Dynamics. Geological Society of London, 83-95.

Cumming, G.L., Richards, J.R., 1975. Ore lead isotope ratios in a continuously changing earth. Earth and Planetary Science Letters, 28, 155-171.

Dias, G., Leterrier, J., Mendes, A., Simoes, P.P., Bertrand, J.M., 1998. U–Pb zircon and monazite geochronology of post-collisional Hercynian granitoids from the Central Iberian Zone (Northern Portugal). Lithos, 45, 349-369.

Dias, G., Simões, P.P., Ferreira, N., Leterrier, J., 2002. Mantle and crustal sources in the genesis of late-Hercynian granitoids (NW Portugal): geochemical and Sr-Nd isotopic constraints. Gondwana Research, 5, 287-305.

Díaz Alvarado, J., Castro, A., Fernández, C., Moreno-Ventas, I., 2011. Assessing bulk assimilation in cordierite-bearing granitoids from the Central System batholith, Spain; experimental, geochemical and geochronological constraints. Journal of Petrology, 52, 223-256.

Díaz Alvarado, J., Fernandez, C., Castro, A., Moreno-Ventas, I., 2013. SHRIMP U-Pb zircon geochronology and thermal modeling of multilayer granitoid intrusions. Implications for the building and thermal evolution of the Central System batholith, Iberian Massif, Spain. Lithos, 175-176, 104-123.

Díez Fernández, R., Pereira, M.F., 2016. Extensional orogenic collapse captured by strike-slip tectonics: Constraints fromstructural geology and U–Pb geochronology of the Pinhel shear zone (Variscan orogen, Iberian Massif). Tectonophysics, 691, 290-310.

Díez Fernández, R., Pereira, M.F., 2017. Strike-slip shear zones of the Iberian Massif: are they coeval? Lithosphere, 9 (5), 726-744.

Díez Fernández, R., Pereira, M.F., Foster, D.A., 2015. Peralkaline and alkaline magmatism of the Ossa-Morena zone (SW Iberia): age, source, and implications for the Paleozoic evolution of Gondwanan lithosphere. Lithosphere, 7, 73-92.

Díez Fernández, R., Arenas, R., Pereira, M.F., Sánchez Martínez, S., Albert, R., Martín Parra, L.M., Rubio Pascual, F.J., Matas, J., 2016. Tectonic evolution of Variscan Iberia: Gondwana-Laurussia collision revisited. Earth Science Reviews, 162, 269-292.

Druguet, E., Castro, A., Chichorro, M., Pereira, M.F., Fernández, C., 2014. Zircon geochronology of intrusive rocks from Cap de Creus, Eastern Pyrenees. Geological Magazine, 151(6), 1095-1114.

Escuder Viruete, J., Arenas, R., Martínez Catalán, J.R., 1994. Tectonothermal evolution associated with Variscan crustal extension in the Tormes Gneiss Dome (NW Salamanca, Iberian Massif, Spain). Tectonophysics, 238, 1-22.

Fernández-Suárez, J., Dunning, G.R., Jenner, G.A., Gutiérrez-Alonso, G., 2000. Variscan collisional magmatism and deformation in NW Iberia: constraints from U-Pb geochronology of granitoids. Journal of the Geological Society, 157, 565-576.

Fernández-Suárez, J., Gutiérre-Alonso, G., Johnston, S.T., Jeffries, T.E., Pastor-Galan, D., Jenner, G.A., Murphy, J.B., 2011. Iberian late-Variscan granitoids: Some considerations on crustal sources and the significance of "mantle extraction ages". Lithos, 123, 121-132.

Ferreira, N., Iglesias Ponce de León, M., Noronha, F., Ribeiro, A., Ribeiro, M.L., 1987. Granitóides da Zona Centro Ibérica e seu enquadramento geodinâmico. In: Bea, F., Carnicero, A., Gonzalo, J.C., López-Plaza, M., Rodríguez Alonso, M.D. (eds.). Geología de los granitoides y rocas asociadas del Macizo Hespérico. Libro Homenaje a L.C. García de Figuerola. Ediciones Rueda, Madrid, 542pp.

Frost, B.R., Barnes, C.G., Collins, W.J., Arculus, R.J., Ellis, D.J. Frost, C.D., 2001. A Geochemical Classification for Granitic Rocks. Journal of Petrology, 42(11), 2033-2048.

Gerya, T.V., Meilick, F.I., 2011. Geodynamic regimes of subduction under an active margin: Effects of rheological weakening by fluids and melts. Journal of Metamorphic Geology, 29, 7-31.

Gerya, T.V., Yuen, D.A., Sevre, E.O.D., 2004. Dynamical causes for incipient magma chambers above slabs. Geology, 32, 89-92.

Gonçalves, F., 1971. Subsídios para o conhecimento geológico do Nordeste Alentejano. Memórias dos Serviços Geológicos de Portugal, 18, 62pp. [In Portuguese]

Gonçalves, F., Coelho, A.V.P., 1969-1970. Nota prévia sobre o provável carácter subvulcânico do maciço granítico de Santa Eulália (Alto Alentejo). Boletim do Museu e Laboratório de Mineralogia e Geologia da Faculdade de Ciências, 11(2), 251-263. [In Portuguese]

Gonçalves, F., Assunção, C.F.T., 1970. Carta Geológica de Portugal na escala 1:50,000. Notícia Explicativa da Folha 37-A, Elvas: Lisboa, Portugal, Serviços Geológicos de Portugal, 50pp. [In Portuguese]

Gonçalves, F., Assunção, C.F.T., Coelho, A.V.P., 1972. Carta Geológica de Portugal na escala 1:50,000. Notícia Explicativa da Folha 33-C, Campo Maior: Lisboa, Portugal, Serviços Geológicos de Portugal, 41pp.

Gonçalves, F., Fernandes, A.P., 1973. Carta Geológica de Portugal na escala 1:50000. Notícia Explicativa da Folha 32-B, Portalegre: Lisboa, Portugal, Serviços Geológicos de Portugal, 45pp.

Gonçalves, F., Zbyszewsky, G., Coelho, A.V.P., 1975. Carta Geológica de Portugal na escala 1:50000. Notícia Explicativa da Folha 32-D, Sousel: Lisboa, Portugal, Serviços Geológicos de Portugal, 49pp.

González Menéndez, L., 2002. Petrología del batolito granítico de Nisa-Alburquerque. Revista de la Sociedad Geológica de España, 15(3-4), 233-246.

González Menéndez, L., Azor, A., Acosta, A., 2002. Estudio petrológico del batolito de Santa Eulália-Monforte (Alto Alentejo, Portugal). Geogaceta, 32, 147-150.

González Menéndez, L., Azor, A., Pereira, M.D., Acosta, A., 2006. Petrogénesis del plutón de Santa Eulália (Alto Alentejo, Portugal). Revista de la Sociedad Geológica de España, 19(1-2), 69-86.

Gutiérrez-Alonso, G., Fernández-Suárez, J., Weil, A.B., Murphy, J.B., Nance, R.D., Corfu, F., Johnston, S.T., 2008. Self-subduction of the Pangaean global plate. Nature Geoscience, 1(8), 549–553.

Gutiérrez-Alonso, G., Fernández-Suárez, J., Jeffries, T.E., Johnston, S.T., Pastor-Galán, D., Murphy, J.B., Piedad Franco, M., Gonzalo, J.C., 2011. Diachronous post-orogenic magmatism within a developing orocline in Iberia, European Variscides. Tectonics, 30(5), TC5008, DOI:10.1029/2010TC002845

Hanchar, J.M., Miller, C.F., 1993. Zircon zonation patterns as revealed by cathodoluminescence and backscattered electron images: implications for interpretation of complex crustal histories. Chemical Geology, 110, 1-13.

Heaman, L.M., Bowins, R., Crocket, J., 1990. The chemical composition of igneous zircon studies: implications for geochemical tracer studies. Geochimica et Cosmochimica Acta, 64, 1905-1923.

Hoskin, P.W.O., Schaltegger, U., 2003. The composition of zircon and igneous and metamorphic petrogenesis. Reviews in Mineralogy and Geochemistry, 53, 27-62.

Jesus, A., Munhá, J., Mateus, A., Tassinari, C., Nutman, A., 2007. The Beja layered gabbroic sequence (Ossa-Morena Zone, Southern Portugal): geochronology and geodynamic implications. Geodinamica Acta, 20, 139-157.

Johnston, S.T., Weil, A.B., Gutiérrez-Alonso, G., 2013. Oroclines, Thick and thin. Gelogical Society of America(GSA) Bulletin 125(5-6), 643-663.

Larrea, F.J., Carracedo, M., Alonso Olazabal, A., Donaire, T., Pascual, E., 2004. El batolito de Los Pedroches. In: Vera, J.A. (ed.). Geología de España. Ediciones de la. Sociedad Geológica de España (SGA) - Instituto Geológico y Minero de España (IGME), Madrid, 122-124.

Lee, C.-T.A., Morton, D.M., Kistler, R.W., Baird, A.K., 2007. Petrology and tectonics of phanerozoic continent formation: From island arcs to accretion and continental arc magmatism. Earth and Planetary Science Letters, 263, 370-387.

Lima, S.M., Corfu, F., Neiva, A.M.R., Ramos, M.F., 2011. Dissecting Complex Magmatic Processes: an in-depth U-Pb Study of the Pavia Pluton, Ossa-Morena Zone, Portugal. Journal of Petrology, 53, 1887-1911.

Lima, S.M., Corfu, F., Neiva, A.M.R., Ramos, M.F., 2012. Dissecting complex magmatic processes: an in-depth U-Pb Study of the Pavia Pluton, Ossa-Morena Zone, Portugal. Journal of Petrology, 53(9), 1887-1911.

Linnemann, U., Pereira, M.F., Jeffreis, T., Drost, K., Gerdes, A., 2008. Cadomian Orogeny and the opening of the Rheic Ocean: New insights in the diacrony of geotectonic processes constrained by LA-ICP-MS U-Pb zircon dating (Ossa-Morena and Saxo-Thuringian Zones, Iberian and Bohemian Massifs). Tectonophysics, 461, 21-43.

López Moro, F.J., López-Plaza, M., Gutiérrez-Alonso, G., Fernández-Suárez, F., López-Carmona, A., Hofmann, M., Romer, R.L., 2017. Crustal melting and recycling: geochronology and sources of Variscan syn-kinematic anatectic granitoids of the Tormes Dome (Central Iberian Zone). A U-Pb LA-ICP-MS study. International Journal of Earth Sciences (Geologische Runbschaw), 1-20, DOI: 10.1007/s00531-017-1483-8.

Ludwig, K.R., 2009. Squid 2.50: a User's Manual Berkeley Geochronology Center, Berkeley, California, USA, 95pp.

Martínez Catalán, J.R., Arenas, R., Abati, J., Sanchéz Martínez, S., Díaz Garcia, F., Fernández-Suárez, J., González Cuadra, P., Castineiras, P., Gomez Barreiro, J., Díez Montes,A., Clavijo, E., Pascual, F.J., Andonaegui, P., Jeffries, T.E., Alcock, J.E., Díez Fernández, R., López Carmona, A., 2009. A rootless suture and the loss of the roots of a mountain chain: the Variscan Belt of NW Iberia. Comptes Rendus Geoscience, 341, 114-126.

Martínez Catalán, J.R., Rubio Pascual, F.J., Díez Montes, A., Díez Fernández, R., Gómez Barreiro, J., Dias da Silva, Í., González Clavijo, E., Ayarza, P., Alcock, J.E., 2014. The late Variscan HT/LP metamorphic event in NW and Central Iberia: relationships to crustal thickening, extension, orocline development and crustal evolution. Geological Society of London, Special Publication, 405, 225-247.

Mendes, F., 1967-1968. Contribution à l'étude géochronologique, par la méthode au strontium, des formations cristallines du Portugal. Boletim Museu e. Laboratório de Mineralogia e Geologia da Faculdade de Ciências da Universidade de Lisboa, 11(1), 3-155.

Merino Martínez, E., Villaseca, C., Orejana, D., Pérez-Soba, C., Belousova, E., Andersen, T., 2014. Tracing magma sources of three different S-type peraluminous granitoid series by in situ U-Pb geochronology and Hf isotope zircon composition: the Variscan Montes de Toledo batholith (central Spain). Lithos, 200-201, 273-298.

Miller, J.S., Matzel, J.E.P., Miller, C.F., Burgess, S.D., Miller, R.B., 2007. Zircon growth and recycling during assembly of large composite arc plutons. Journal of Volcanology and Geothermal Research, 167, 282-299.

Moita, P., Santos, J.F., Pereira, M.F., 2009. Layered granitoids: interaction between continental crust recycling processes and mantle-derived magmatism. Examples from the Évora Massif (Ossa-Morena Zone, southwest Iberia, Portugal). Lithos, 111(3-4), 125-141.

Moita, P., Santos, J.F., Pereira, M.F., Costa, M.M., Corfu, F., 2015. The quartz-dioritic Hospitais intrusion (SW Iberian Massif) and its mafic microgranular enclaves - evidence for mineral clustering. Lithos, 224-225, 78-100.

Montero, P., Bea, F., Zinger, T.F., Scarrow, J.H., Molina, J.F., Whitehouse, M., 2004. 55 million years of continuous antexis in Central Iberia: single-zircon dating of the Peña Negra Complex. Journal of the Geological Society of London, 161, 255-263.

Montero, P., Bea, F., Corretgé, L.G., Floor, P., Whitehouse, M.J., 2008. U-Pb ion microprobe dating and Sr-Nd isotope geology of the Galiñeiro Igneous Complex. A model for the peraluminous/peralkaline duality of the Cambro-Ordovician magmatism of Iberia. Lithos, 107, 227-238.

Murphy, J.B., 2013. Appinite suites: A record of the role of water in the genesis, transport, emplacement and crystallization of magma. Earth Science Reviews, 119, 35-59.

Neiva, A.M.R., Gomes M.E.P., 2001. Diferentes tipos de granitos e seus processos petrogenéticos: Granitos Hercínicos Portugueses. Memórias da Academia das Ciências de Lisboa XXXIX, 53-95.

Neiva, A. M. R., Williams, I.S., Ramos, J.M.F., Gomes, M.E.P., Silva, M.M.V.G., Antunes, I.M.H.R., 2009. Geochemical and isotopic constraints on the petrogenesis of Early Ordovician granodiorite and Variscan two-mica granites from the Gouveia area, central Portugal, Lithos, 111, 186-202.

Neiva, A.M.R., Williams, I.S., Lima, S.M., Teixeira, R.J.S., 2012. U-Pb and $^{39}Ar/^{40}Ar$ data constraining the ages of the source, emplacement and recrystallization/cooling events from late- to post-D_3 Variscan granites of the Gouveia area, central Portugal. Lithos, 153, 72-83.

Oliveira, V.M.J., 1975. Cartografia inédita do granito de Santa Eulália (anéis G1, G2 e G3). Unpublished map. Serviço de Fomento Mineiro da Direcção Geral de Geologia e Minas, Portugal.

Oliveira, J.T., Oliveira, V.M.J., Piçarra, J.M., 1991. Traços gerais da evolução tectonoestratigráfica da zona de Ossa Morena, em Portugal: Síntese crítica do estado actual dos conhecimentos. Comunicações dos Serviços Geológicos de Portugal, 77, 3-26.

Orejana, D., Villaseca, C., Valverde-Vaquero, P., Belousova, E.A., Armstrong, R.A., 2012. U-Pb geochronology and zircon composition of late Variscan S- and I-type granitoids from the Spanish Central System. International Journal of Earth Sciences. DOI:10.1007/s00531-012-0750-y

Pereira, M.F., 1999. Caracterização da estrutura dos domínios setentrionais da Zona de Ossa-Morena e seu limite com a Zona Centro-Ibérica, no nordeste Alentejano. Unpublished PhD Thesis, Universidade de Évora, 115pp.

Pereira, M.F., Quesada, C., 2006. Ediacaran to Visean crustal growth processes in the Ossa-Morena zone (SW Iberia), International Geoscience Programme 497 Évora Meeting 2006. Conference Abstracts and Field Trip Guide: Madrid, Spain, Publicaciones IGME, 115pp.

Pereira, M.F., Chichorro, M., Linnemann, U., Eguiluz, L., and Silva, J.B., 2006. Inherited arc signature in Ediacaran and Early Cambrian basins of the Ossa-Morena zone (Iberian Massif, Portugal): Paleogeographic link with European and North African Cadomian correlatives. Precambrian Research, 144, 297-315.

Pereira, M.F., Apraiz, A., Silva, J.B., and Chichorro, M., 2008. Tectonothermal analysis of high temperature mylonitization in the Coimbra-Cordoba shear zone (SW Iberian Massif, Ouguela tectonic unit, Portugal) Evidence of intra-continental transcurrent transport during the amalgamation of Pangea. Tectonophysics, 461, 378-394.

Pereira, M.F., Chichorro, M., Williams, I.S., Silva, J.B., Fernandez, C., Diaz-Azpiroz, M., Apraiz, A., Castro, A., 2009. Variscan intra-orogenic extensional tectonics in the Ossa-Morena Zone (Évora-Aracena-Lora del Rio metamorphic belt, SW Iberian Massif): SHRIMP zircon U–Th–Pb geochronology. In: Murphy, J.B., Keppie, J.D., Hynes, A.J. (eds.). Ancient Orogens and Modern Analogues. Geological Society of London, Special Publications 327, 215-237.

Pereira, M.F., Apraiz, A., Chichorro, M., Silva, J.B., Armstrong, R.A., 2010. Exhumation of high-pressure rocks in northern Gondwana during the early Carboniferous (Coimbra-Cordoba shear zone, SW Iberian Massif): Tectonothermal analysis and U-Th-Pb SHRIMP in-situ zircon geochronology. Gondwana Research, 17, 440-460.

Pereira, M.F., Chichorro, M., Solá, A.R., Silva, J.B., Sánchez-García, T., Bellido, F., 2011. Tracing the Cadomian magmatism with detrital/inherited zircon ages by in-situ U-Pb SHRIMP geochronology (Ossa-Morena zone, SW Iberian Massif). Lithos, 123, 204-217.

Pereira, M.F., Chichorro, M., Silva, J.B., Ordonez-Casado, B., Lee, J.K.W., Williams, I.S., 2012. Early Carboniferous wrenching, exhumation of high-grade metamorphic rocks and basin instability in SW Iberia: Constraints derived from structural geology and U–Pb and $^{40}Ar/^{39}Ar$ geochronology. Tectonophysics, 558-559, 28-44.

Pereira, M.F., Castro, A., Chichorro, C., Fernández, C., Díaz-Alvarado, J. Martí, J., Rodríguez, C., 2014. Chronological link between deep-seated processes in magma chambers and eruptions: Permo-Carboniferous magmatism in the core of Pangaea (Southern Pyrenees). Gondwana Research, 25, 290-308.

Pereira, M.F., Chichorro, M., Moita, P., Santos, J.F., Solá, A.M.R., Williams, I.S., Silva, J.B., Armstrong, R.A., 2015a. The multistage crystallization of zircon in calc-alkaline granitoids: U-Pb age constraints on the timing of Variscan tectonic activity in SW Iberia. International Journal of Earth Sciences. http://dx.DOI.org/10.1007/s00531-015-1149-3.

Pereira, M.F., Castro, A., Fernández, C., 2015b. The inception of a Paleotethyan magmatic arc in Iberia. Geosciences Frontiers, 6, 297-306.

Pereira, M.F., Díez Fernández, R., Gama, C., Hofmann, M., Gärtner, A., Linnemann, U., 2017a. S-type granite generation and emplacement during a regional switch from extensional to contractional deformation (Central Iberian Zone, Iberian autochthonous domain, Variscan Orogeny). International Journal of Earth Sciences, DOI: 10.1007/s00531-017-1488-3.

Pereira, M. F., Gutíerrez-Alonso, G., Murphy, J. B., Drost, K., Gama, C., Silva, J. B., 2017b. Birth and demise of the Rheic Ocean magmatic arc(s): Combined U-Pb and Hf isotope analyses in detrital zircon from SW Iberia siliciclastic strata. Lithos, 278-281, 383-399.

Pin, C., Fonseca, P.E., Paquette, J.L., Castro, P., Matte, Ph., 2008. The *ca*. 350Ma Beja igneous complex: a record of transcurrent slab break-off in the southern Iberia Variscan Belt? Tectonophysics, 461, 356-377.

Pinto, M.S., Casquet, C., Ibarrola, E., Corretgé, L.G., Ferreira, M.P., 1987. Síntese geocronológica dos granitóides do Maciço Hespérico. In: Bea, F., Carnicero, A., Gonzalo, J.C., López Plaza, M., Rodríguez Alonso, M.D. (eds.). Geología de los granitoides y rocas associadas del Macizo Hespérico, Libro de Homenaje a L. C. García de Figuerola. Editorial Rueda, Madrid, 69-86pp.

Roberts, M.P., Pin, C., Clemens, J.D., Paquette, J.L., 2000. Petrogenesis of mafic to felsic plutonic rock associations: the calc-alkaline Quérigut complex, French Pyrenees. Journal of Petrology, 41, 809-844.

Sánchez-García, T., Bellido, F., Pereira, M.F., Chichorro, M., Quesada, C., Pin, C., Silva, J.B., 2010. Rift-related volcanism predating the birth of the Rheic Ocean (Ossa-Morena zone, SW Iberia). Gondwana Research, 17, 392-407.

Sánchez-García, T., Pereira, M.F., Bellido, F., Chichorro, M., Silva, J.B., Valverde-Vaquero, P., Pin, C., Solá, A.R., 2013. Early Cambrian granitoids of North Gondwana margin in the transition from a convergent setting to intra-continental rifting (Ossa-Morena zone, SW Iberia). International Journal of Earth Sciences, 103, 1203-1218.

Sant'Ovaia, H., Nogueira, P., Carrilho Lopes, J., Gomes, C., Ribeiro, M.A., Martins, H.C.B., Dória, A., Cruz, C., Lopes, L., Sardinha, R., Rocha, A., Noronha, F., 2015. Building up of a nested granite intrusion: magnetic fabric, gravity modelling and fluid inclusion planes studies in Santa Eulália Plutonic Complex (Ossa Morena Zone, Portugal). Geological Magazine, 152 (4), 648-667.

Simancas, J.F., Tahiri, A., Azor, A., Lodeiro, F.G., Poyatos, D.J.M., Hadi, H.E., 2005. The tectonic frame of the Variscan–Alleghanian orogen in southern Europe and northern Africa. Tectonophysics, 98, 181-198.

Solá, A.R., Williams, I.S., Neiva, A.M.R., Ribeiro, M.L., 2009. U–Th–Pb SHRIMP ages and oxygen isotope composition of zircon from two contrasting late Variscan granitoids, Nisa-Albuquerque batholith, SW Iberian Massif: Petrologic and regional implications. Lithos, 111, 156-167.

Solé, J., Cosca, M., Sharp, Z., Enrique, P., 2002. $^{40}Ar/^{39}Ar$ geochronology and stable isotope geochemistry of late-Hercynian intrusions from north-eastern Iberia with implications for argon loss in K-feldspar. International Journal of Earth Sciences, 91, 865-881.

Stampfli, G.M., Borel, G.D., 2002. A plate tectonic model for the Paleozoic and Mesozoic constrained by dynamic plate boundaries and restored synthetic oceanic isochrones: Earth and Planetary Science Letters, 196, 17-33

Stampfli, G.M., Kozur, H., 2006. Europe from the Variscan to the Alpine cycles. In: Gee, D.G., Stephenson, R., (eds.). European Lithosphere Dynamics. Geological Society of London Memoir, 32, 57-82.

Stampfli, G.M., Hochard, C., Vérard, C., Wilhem, C., von Raumer, J., 2013. The formation of Pangea. Tectonophysics, 593, 1-19.

Teixeira, R.J.S., Neiva, A.M.R., Silva, P.B., Gomes, M.E.P., Andersen, T., Ramos, J.M.F., 2011. Combined U-Pb geochronology and Lu-Hf isotope systematics by LAM-ICPMS of zircons from granites and metasedimentary rocks of Carrazeda de Ansiães and Sabugal areas, Portugal, to constrain granite sources. Lithos, 125, 321-334.

Turnbull, R., Weaver, S., Tulloch, A., Cole, J., Handler, M., Ireland, T., 2010. Field and geochemical constraints on mafic-felsic interactions, and processes in high-level arc magma chambers: an example from the Halfmoon Pluton, New Zealand. Journal of Petrology, 51(7), 1477-1505.

Valle Aguado, B., Azevedo, M.R., Schaltegger, U., Martínez Catalán, J.R., Nolan, J., 2005. U-Pb zircon and monazite geochronology of Variscan magmatism related to synconvergence extension in Central Northern Portugal. Lithos, 82, 169-184.

Valverde-Vaquero, P., 1997. An integrated field, geochemical and U-Pb geochronological study of the southwest Hermitage Flexure (Newfoundland Appalachians, Canada) and the Sierra De Guadarrama (Iberian Massif, Central Spain): a contribution to the understanding of the geological evolution of circum- Atlantic Peri-Gondwana. Unpublished PhD Thesis. Memorial University of Newfoundland, 312pp.

Valverde-Vaquero, P., Bento dos Santos, T., Clavijo, E.G., Díez Montes, A., Ribeiro, M.L., Solá, A.R., Dias da Silva, Í., 2011. The Berlengas Archipelago granitoids within the frame of the Variscan Orogeny, W-Portugal: new data and insights. VII Hutton Symposium on Granites and Related Rocks. Abstracts Book, Avila, Spain, 131-132.

Villaseca, C., Bellido, F., Pérez-Soba, C., Billström, K., 2009. Multiple crustal sources for post-tectonic I-type granites in the Hercynian Iberian Belt. Mineralogy and Petrology, 96, 197-211.

Villaseca, C., Orejana, D., Belousova, E.A., 2012. Recycled metaigneous crustal sources for S- and I-type Variscan granitoids from the Spanish Central System batholith: constraints from Hf isotope zircon composition. Lithos, 153, 84-93.

Vogt, K., Gerya, T.V., Castro, A., 2012. Crustal growth at active continental margins: Numerical modeling. Physics of the Earth and Planetary Interiors, 192-193. 1-20.

Weil, A., Gutiérrez-Alonso, G., Johnston, S.T., Pastor-Galán, D., 2012. Kinematic constraints on buckling a lithospheric-scale orocline along the northern margin of Gondwana: A geologic synthesis. Tectonophysics, 582, 25-49.

Williams, I.S., 1998. U-Th-Pb Geochronology by Ion Microprobe. In: McKibben, M. A., Shanks III, W. C., Ridley, W. I. (eds.). Applications of microanalytical techniques to understanding mineralizing processes. Reviews in Economic Geology, 7, 1-35.

Williams, I.S., Hergt, J.M., 2000. U-Pb dating of Tasmanian dolerites: a cautionary tale of SHRIMP analysis of high-U zircon. In: J.D. Woodhead, J.M. Hergt, W.P. Noble (eds.). Beyond 2000: new frontiers in isotope science. Lorne, Abstracts and Proceedings, 185-188.

Manuscript received June 2017;
revision accepted November 2017;
published Online November 2017.

ELECTRONIC APPENDIX I

TABLE 1. Zircon U-Pb geochronological data (samples from the external ring of the Santa Eulália-Monforte massif)

id	U (ppm)	Th (ppm)	^{206}Pb (ppm)	% f206_4	% f206_8	Th/U	common lead uncorrected isotope ratios								
							^{204}Pb/^{206}Pb	±err	^{207}Pb/^{206}Pb	±err	^{206}Pb/^{238}U	±err	^{207}Pb/^{235}U	±err	rho
BCA2-1.1	124.8	78.5	5.5	1.2	0.1	0.65	0.00071	0.00017	0.05316	0.00062	0.05075	0.00088	0.37199	0.00779	0.599
BCA2-10.1	144.7	92.4	5.9	0.2	0.0	0.65	0.00014	0.00010	0.05177	0.00049	0.04715	0.00068	0.33651	0.00580	0.601
BCA2-11.1	629.4	343.1	26.8	0.0	-0.1	0.56	0.00000	0.00003	0.05226	0.00026	0.04925	0.00055	0.35487	0.00434	0.659
BCA2-12.1	184.6	125.1	7.4	0.2	-0.5	0.70	0.00009	0.00009	0.05041	0.00082	0.04649	0.00087	0.32313	0.00798	0.544
BCA2-13.1	244.4	147.1	10.5	1.1	-0.5	0.62	0.00065	0.00060	0.05123	0.00098	0.04972	0.00076	0.35121	0.00858	0.451
BCA2-14.1	115.9	80.5	4.6	0.2	0.3	0.71	0.00012	0.00012	0.05318	0.00031	0.04569	0.00128	0.33498	0.00956	0.705
BCA2-15.1	137.2	53.7	5.7	-0.2	0.0	0.40	-0.00010	0.00010	0.05453	0.00076	0.04833	0.00086	0.36338	0.00821	0.566
BCA2-16.1	232.2	113.0	9.6	0.5	-0.1	0.50	0.00027	0.00009	0.05168	0.00071	0.04769	0.00081	0.33980	0.00743	0.558
BCA2-17.1	281.4	189.4	9.6	0.3	-1.7	0.69	0.00018	0.00014	0.05402	0.00042	0.03937	0.00070	0.29325	0.00572	0.660
BCA2-18.1	218.9	148.6	9.3	3.0	-0.1	0.70	0.00180	0.00167	0.05484	0.00106	0.04886	0.00067	0.36949	0.00877	0.417
BCA2-19.1	156.1	109.2	6.4	-0.1	0.2	0.72	-0.00008	0.00008	0.05188	0.00081	0.04702	0.00075	0.33637	0.00752	0.516
BCA2-2.1	112.8	73.4	4.8	0.4	-0.2	0.67	0.00024	0.00010	0.05174	0.00052	0.04934	0.00078	0.35196	0.00660	0.608
BCA2-20.1	167,4	96.2	7.0	0.5	0.0	0.59	0.00031	0.00010	0.05326	0.00151	0.04854	0.00051	0.35649	0.01076	0.249
BCA2-21.1	265.9	180.1	11.0	0.1	-0.2	0.69	0.00007	0.00005	0.05429	0.00058	0.04772	0.00087	0.35727	0.00756	0.622
BCA2-22.1	319.0	190.0	13.6	-0.2	-0.2	0.61	-0.00011	0.00007	0.05226	0.00070	0.04943	0.00050	0.35617	0.00599	0.433
BCA2-23.1	179.1	113.0	7.4	0.3	0.1	0.65	0.00019	0.00012	0.05222	0.00131	0.04747	0.00079	0.34178	0.01029	0.396
BCA2-24.1	100.5	47.7	4.4	1.3	0.1	0.49	0.00079	0.00016	0.05464	0.00010	0.05034	0.00054	0.37929	0.00414	0.709
BCA2-3.1	220.1	117.3	9.6	0.1	0.0	0.55	0.00007	0.00011	0.05242	0.00019	0.05049	0.00091	0.36497	0.00671	0.705
BCA2-4.1	105.8	65.2	4.4	-0.1	-0.2	0.63	-0.00005	0.00015	0.05245	0.00098	0.04808	0.00072	0.34768	0.00833	0.450
BCA2-5.1	89.1	56.8	3.7	0.3	0.1	0.65	0.00017	0.00011	0.05253	0.00067	0.04859	0.00086	0.35193	0.00765	0.584
BCA2-6.1	244.3	153.5	10.0	0.2	0.3	0.64	0.00014	0.00006	0.05247	0.00113	0.04743	0.00073	0.34318	0.00905	0.417
BCA2-7.1	154.0	99.5	6.5	-0.1	-0.2	0.66	-0.00005	0.00003	0.05245	0.00069	0.04861	0.00080	0.35155	0.00745	0.563
BCA2-8.1	222.0	132.5	9.3	0.1	-0.3	0.61	0.00004	0.00004	0.05226	0.00036	0.04845	0.00089	0.34914	0.00687	0.675
BCA2-9.1	243.9	194.2	10.0	-0.2	-0.2	0.82	-0.00012	0.00005	0.05202	0.00052	0.04722	0.00072	0.33874	0.00616	0.603
MFT1-1.1	574.1	176.5	22.7	0.3	0.2	0.32	0.00016	0.00005	0.05389	0.00044	0.04578	0.00107	0.34014	0.00842	0.679
MFT1-1.2	740.6	216.2	31.0	0.1	0.0	0.30	0.00004	0.00002	0.05374	0.00049	0.04839	0.00114	0.35857	0.00906	0.672

BCA-2- gabbro-diorite (39º4'5.9"N; 7º12'51"W); MFT-1- pinkish granite (39º04'4.5"N; 7º13'53"W)
SHRIMPTOOLS data processing; IBERSIMS laboratory, University of Granada, Spain
Errors are at one sigma level. The error in 206/238 averaging the standard has been already propagated. Th/U ratios are atomic (232/238), not in weight
Point-to point errors, calculated on replicates of the TEMORA standard, are: 0.36% for ^{206}Pb/^{238}U, and 0.32% for ^{207}Pb/^{206}Pb

TABLE 1. (Cont.)

id	U (ppm)	Th (ppm)	^{206}Pb (ppm)	% f206_4	% f206_8	Th/U	common lead uncorrected isotope ratios								
							^{204}Pb/^{206}Pb	±err	^{207}Pb/^{206}Pb	±err	^{206}Pb/^{238}U	±err	^{207}Pb/^{235}U	±err	rho
MFT1-10.1	3246.3	582.4	129.3	0.2	0.1	0.18	0.00014	0.00001	0.05417	0.00013	0.04533	0.00115	0.34364	0.00861	0.727
MFT1-11.1	2277.6	1763.1	94.6	0.0	-0.1	0.79	0.00003	0.00002	0.05286	0.00011	0.04796	0.00097	0.34957	0.00710	0.716
MFT1-12.1	861.8	254.6	35.7	0.7	0.8	0.30	0.00042	0.00005	0.05708	0.00035	0.04785	0.00065	0.37655	0.00561	0.656
MFT1-13.1	879.6	381.2	35.5	0.1	0.0	0.44	0.00007	0.00003	0.05343	0.00018	0.04664	0.00074	0.34364	0.00560	0.705
MFT1-14.1	4891.5	1761.5	194.0	0.6	-2.1	0.37	0.00035	0.00006	0.05720	0.00027	0.04362	0.00231	0.36132	0.01831	0.753
MFT1-15.1	751.7	284.3	30.6	0.1	-0.1	0.39	0.00004	0.00003	0.05155	0.00037	0.04700	0.00089	0.33409	0.00678	0.674
MFT1-16.1	8522.3	657.5	366.2	0.1	0.5	0.08	0.00007	0.00001	0.05374	0.00013	0.04366	0.00160	0.36784	0.01190	0.816
MFT1-17.1	396.7	156.9	16.5	0.1	0.1	0.41	0.00003	0.00007	0.05160	0.00031	0.04795	0.00080	0.34115	0.00604	0.677
MFT1-18.1	913.7	359.4	35.1	0.1	0.1	0.40	0.00008	0.00004	0.05349	0.00016	0.04443	0.00140	0.32773	0.01035	0.717
MFT1-18.2	7013.1	5433.9	219.4	7.2	2.1	0.79	0.00425	0.00015	0.11705	0.00212	0.03288	0.00146	0.58321	0.02589	0.722
MFT1-19.1	1092.1	315.4	45.2	0.6	0.5	0.30	0.00037	0.00008	0.05556	0.00029	0.04778	0.00137	0.36599	0.01064	0.709
MFT1-19.2	911.8	406.1	34.5	8.8	10.9	0.46	0.00518	0.00024	0.13192	0.00209	0.04373	0.00112	0.79539	0.02394	0.612
MFT1-20.1	634.7	218.4	24.9	0.0	0.2	0.35	-0.00002	0.00003	0.05317	0.00024	0.04527	0.00182	0.33190	0.01342	0.715
MFT1-21.1	172.1	57.1	6.9	0.6	-0.2	0.34	0.00035	0.00006	0.05155	0.00026	0.04627	0.00115	0.32881	0.00835	0.705
MFT1-22.1	844.4	299.3	35.2	0.1	0.1	0.36	0.00006	0.00004	0.05278	0.00022	0.04821	0.00138	0.35083	0.01015	0.712
MFT1-23.1	186.1	69.5	8.9	13.7	15.5	0.38	0.00811	0.00215	0.16428	0.02318	0.05523	0.00129	1.25107	0.17891	0.117
MFT1-24.1	893.8	394.4	37.0	0.0	-0.1	0.45	0.00001	0.00001	0.05296	0.00016	0.04781	0.00105	0.34913	0.00774	0.713
MFT1-24.2	295.8	117.5	13.3	11.0	11.7	0.41	0.00647	0.00033	0.14489	0.00332	0.05207	0.00118	1.04012	0.03351	0.507
MFT1-25.1	365.8	121.2	15.1	0.1	0.1	0.34	0.00005	0.00003	0.05212	0.00032	0.04769	0.00072	0.34273	0.00556	0.667
MFT1-3.1	6604.7	822.0	232.9	1.7	1.8	0.13	0.00099	0.00019	0.06876	0.00296	0.03740	0.00164	0.38627	0.02278	0.537
MFT1-4.1	6165.8	1616.6	206.5	2.8	3.9	0.27	0.00166	0.00016	0.08012	0.00308	0.03585	0.00179	0.42740	0.02572	0.598
MFT1-5.1	726.5	328.9	31.8	0.0	-0.1	0.46	-0.00002	0.00003	0.05332	0.00040	0.05054	0.00203	0.37160	0.01516	0.708
MFT1-6.1	574.4	190.3	23.7	0.3	0.1	0.34	0.00017	0.00002	0.05384	0.00049	0.04763	0.00081	0.35354	0.00683	0.636
MFT1-7.1	1141.6	372.1	46.5	1.0	1.2	0.33	0.00058	0.00008	0.06071	0.00024	0.04705	0.00127	0.39383	0.01071	0.712
MFT1-8.1	1719.5	578.6	71.1	0.6	0.3	0.35	0.00035	0.00003	0.05666	0.00018	0.04777	0.00145	0.37322	0.01135	0.716
MFT1-8.2	2885.0	893.3	218.6	0.1	-0.2	0,32	0.00005	0.00001	0.05916	0.00024	0.08687	0.00862	0.71414	0.07041	0.725
MFT1-9.1	1078.1	512.2	45.1	1.0	0.7	0.49	0.00058	0.00008	0.06180	0.00064	0.04837	0.00172	0.41219	0.01530	0.691

BCA-2- gabbro-diorite (39º4'5.9"N; 7º12'51"W); MFT-1- pinkish granite (39º04'4.5"N; 7º13'53"W)
SHRIMPTOOLS data processing; IBERSIMS laboratory, University of Granada, Spain
Errors are at one sigma level. The error in 206/238 averaging the standard has been already propagated. Th/U ratios are atomic (232/238), not in weight
Point-to point errors, calculated on replicates of the TEMORA standard, are: 0.36% for ^{206}Pb/^{238}U, and 0.32% for ^{207}Pb/^{206}Pb

TABLE 1. (Cont.)

			common lead uncorrected ages (Ma)						
id	**$^{208}Pb/^{232}Th$**	**±err**	**$^{207}Pb/^{206}Pb$**	**±err**	**$^{206}Pb/^{238}U$**	**±err**	**$^{207}Pb/^{235}U$**	**±err**	**% discord.**
BCA2-1.1	0.01607	0.00036	335.5	26.2	319.1	5.4	321.1	5.8	0.6
BCA2-10.1	0.01474	0.00023	275.1	21.6	297.0	4.2	294.5	4.4	-0.8
BCA2-11.1	0.01535	0.00018	296.7	11.2	309.9	3.4	308,4	3.3	-0.4
BCA2-12.1	0.01403	0.00032	213.9	37.0	292.9	5.3	284.3	6.1	-3.0
BCA2-13.1	0.01481	0.00041	251.1	43.2	312.8	4.6	305.6	6.4	-2.4
BCA2-14.1	0.01469	0.00076	336.5	12.8	288.0	7.9	293.4	7.3	1.8
BCA2-15.1	0.01516	0.00031	392.9	31.0	304.3	5.3	314.7	6.1	3.4
BCA2-16.1	0.01483	0.00030	271.1	31.4	300.3	4.9	297.0	5.6	-1.2
BCA2-17.1	0.01061	0.00022	371.7	17.6	249.0	4.4	261.1	4.5	4.6
BCA2-18.1	0.01523	0.00024	405.9	42.8	307.5	4.1	319.3	6.6	3.6
BCA2-19.1	0.01504	0.00026	280.1	35.4	296.2	4.6	294.4	5.7	-0.6
BCA2-2.1	0.01527	0.00030	273.9	22.8	310.5	4.8	306.2	5.0	-1.4
BCA2-20.1	0.01530	0.00024	340.1	62.8	305.6	3.1	309.6	8.1	1.2
BCA2-21.1	0.01475	0.00029	383.3	23.8	300.5	5.3	310.2	5.7	3.2
BCA2-22.1	0.01522	0.00018	296.7	30.4	311.0	3.0	309.3	4.4	-0.6
BCA2-23.1	0.01507	0.00032	295.1	56.4	299.0	4.9	298.5	7.8	-0.2
BCA2-24.1	0.01601	0.00028	397.7	4.2	316.6	3.3	326.5	3.0	3.0
BCA2-3.1	0.01586	0.00032	303.9	8.4	317.5	5.5	315.9	5.0	-0.6
BCA2-4.1	0.01484	0.00036	305.1	42.0	302.7	4.4	303.0	6.3	0.0
BCA2-5.1	0.01533	0.00038	308.5	28.8	305.9	5.3	306.2	5.8	0.0
BCA2-6.1	0.01527	0.00026	306.1	48.2	298.8	4.5	299.6	6.9	0.2
BCA2-7.1	0.01494	0.00033	304.9	30.0	306.0	4.9	305.9	5.6	0.0
BCA2-8.1	0.01479	0.00032	296.9	15.4	305.0	5.5	304.1	5.2	-0.2
BCA2-9.1	0.01467	0.00024	286.5	22.6	297.5	4.5	296.2	4.7	-0.4
MFT1-1.1	0.01508	0.00038	366.5	18.4	288.5	6.6	297.3	6.4	3.0
MFT1-1.2	0.01526	0.00060	360.3	20.4	304.6	7.0	311.1	6.7	2.0
MFT1-10.1	0.01516	0.00046	377.9	5.6	285.8	7.1	299.9	6.5	4.8

BCA-2- gabbro-diorite (39º4'5.9"N; 7º12'51"W); MFT-1- pinkish granite (39º04'4.5"N; 7º13'53"W)
SHRIMPTOOLS data processing; IBERSIMS laboratory, University of Granada, Spain
Errors are at one sigma level. The error in 206/238 averaging the standard has been already propagated. Th/U ratios are atomic (232/238), not in weight
Point-to point errors, calculated on replicates of the TEMORA standard, are: 0.36% for $^{206}Pb/^{238}U$, and 0.32% for $^{207}Pb/^{206}Pb$

TABLE 1. (Cont.)

	common lead uncorrected ages (Ma)								
id	**$^{208}Pb/^{232}Th$**	**±err**	**$^{207}Pb/^{206}Pb$**	**±err**	**$^{206}Pb/^{238}U$**	**±err**	**$^{207}Pb/^{235}U$**	**±err**	**% discord.**
MFT1-11.1	0.01492	0.00033	322.9	4.4	302.0	6.0	304.4	5.4	0.8
MFT1-12.1	0.01764	0.00026	494.5	13.4	301.3	4.0	324.5	4.1	7.2
MFT1-13.1	0.01459	0.00027	347.3	7.6	293.9	4.6	299.9	4.2	2.0
MFT1-14.1	0.00921	0.00071	499.3	10.4	275.2	14.3	313.2	13.7	12.2
MFT1-15.1	0.01458	0.00031	265.5	16.4	296.1	5.5	292.7	5.2	-1.2
MFT1-16.1	0.02197	0.00185	360.3	5.4	275.5	9.9	318.1	8.9	13.4
MFT1-17.1	0.01526	0.00027	267.9	13.8	301.9	4.9	298.0	4.5	-1.4
MFT1-18.1	0.01423	0.00046	349.7	6.6	280.3	8.7	287.8	7.9	2.6
MFT1-18.2	0.01316	0.00068	1911.7	32.2	208.5	9.1	466.5	16.7	55.4
MFT1-19.1	0.01676	0.00049	434.9	11.4	300.9	8.5	316.7	8.0	5.0
MFT1-19.2	0.03406	0.00105	2123.7	27.4	275.9	6.9	594.2	13.6	53.6
MFT1-20.1	0.01468	0.00073	336.3	10.4	285.4	11.2	291.0	10.3	2.0
MFT1-21.1	0.01408	0.00039	265.3	11.8	291.6	7.1	288.7	6.4	-1.0
MFT1-22.1	0.01543	0.00044	319.5	9.6	303.5	8.5	305.3	7.6	0.6
MFT1-23.1	0.06126	0.00763	2500.3	219.8	346.6	7.9	823.9	84.1	58.0
MFT1-24.1	0.01486	0.00034	326.9	6.8	301.1	6.5	304.1	5.9	1.0
MFT1-24.2	0.04562	0.00147	2286.5	38.8	327.2	7.2	724.0	16.8	54.8
MFT1-25.1	0.01538	0.00032	290.7	13.8	300.3	4.4	299.2	4.2	-0.4
MFT1-3.1	0.02475	0.00301	891.7	86.4	236.7	10.2	331.6	16.8	28.6
MFT1-4.1	0.02358	0.00231	1200.1	74.0	227.1	11.2	361.3	18.4	37.2
MFT1-5.1	0.01569	0.00070	342.5	17.0	317.8	12.4	320.8	11.2	1.0
MFT1-6.1	0.01532	0.00028	364.3	20.2	299.9	5.0	307.4	5.2	2.4
MFT1-7.1	0.01818	0.00050	629.1	8.6	296.4	7.8	337.2	7.9	12.0
MFT1-8.1	0.01572	0.00050	478.3	7.0	300.8	8.9	322.0	8.4	6.6
MFT1-8.2	0.02607	0.00353	573.1	8.8	537.0	51.4	547.2	42.6	1.8
MFT1-9.1	0.01645	0.00070	667.3	22.0	304.5	10.6	350.4	11.0	13.0

BCA-2- gabbro-diorite (39º4'5.9"N; 7º12'51"W); MFT-1- pinkish granite (39º04'4.5"N; 7º13'53"W)
SHRIMPTOOLS data processing; IBERSIMS laboratory, University of Granada, Spain
Errors are at one sigma level. The error in 206/238 averaging the standard has been already propagated. Th/U ratios are atomic (232/238), not in weight
Point-to point errors, calculated on replicates of the TEMORA standard, are: 0.36% for $^{206}Pb/^{238}U$, and 0.32% for $^{207}Pb/^{206}Pb$

TABLE 1. (Cont.)

			204-corrected isotope ratios						
id	$^{208}Pb/^{232}Th$	**±err**	$^{207}Pb/^{206}Pb$	**±err**	$^{206}Pb/^{238}U$	**±err**	$^{207}Pb/^{235}U$	**±err**	**rho_4cor**
BCA2-1.1	322.1	7.2	0.04254	0.00284	0.05009	0.00089	0.29377	0.02035	0.184
BCA2-10.1	295.8	4.6	0.04971	0.00163	0.04703	0.00068	0.32231	0.01164	0.289
BCA2-11.1	308.0	3.6	0.05229	0.00052	0.04925	0.00055	0.35509	0.00548	0.523
BCA2-12.1	281.6	6.4	0.04910	0.00163	0.04641	0.00087	0.31422	0.01203	0.352
BCA2-13.1	297.1	8.2	0.04162	0.00960	0.04914	0.00093	0.28201	0.06527	0.059
BCA2-14.1	294.7	15.1	0.05143	0.00187	0.04559	0.00128	0.32328	0.01491	0.438
BCA2-15.1	304.1	6.1	0.05602	0.00177	0.04842	0.00087	0.37401	0.01362	0.353
BCA2-16.1	297.5	6.1	0.04772	0.00154	0.04746	0.00081	0.31227	0.01148	0.334
BCA2-17.1	213.4	4.5	0.05142	0.00223	0.03925	0.00071	0.27825	0.01309	0.276
BCA2-18.1	305.4	4.7	0.02760	0.02707	0.04725	0.00163	0.17978	0.17649	0.025
BCA2-19.1	301.6	5.2	0.05308	0.00153	0.04709	0.00076	0.34470	0.01142	0.349
BCA2-2.1	306.3	6.0	0.04823	0.00172	0.04912	0.00078	0.32667	0.01284	0.292
BCA2-20.1	306.8	4.7	0.04866	0.00220	0.04826	0.00051	0.32380	0.01509	0.164
BCA2-21.1	296.0	5.7	0.05321	0.00095	0.04766	0.00087	0.34967	0.00902	0.511
BCA2-22.1	305.4	3.7	0.05385	0.00136	0.04953	0.00050	0.36779	0.01010	0.267
BCA2-23.1	302.3	6.4	0.04945	0.00232	0.04730	0.00079	0.32253	0.01612	0.241
BCA2-24.1	320.9	5.6	0.04293	0.00255	0.04962	0.00055	0.29369	0.01780	0.132
BCA2-3.1	318.0	6.4	0.05141	0.00178	0.05043	0.00091	0.35747	0.01405	0.332
BCA2-4.1	297.7	7.2	0.05317	0.00248	0.04812	0.00073	0.35276	0.01737	0.222
BCA2-5.1	307.4	7.5	0.05007	0.00187	0.04844	0.00086	0.33444	0.01390	0.308
BCA2-6.1	306.2	5.3	0.05046	0.00146	0.04732	0.00073	0.32923	0.01084	0.335
BCA2-7.1	299.7	6.5	0.05321	0.00087	0.04866	0.00081	0.35700	0.00839	0.508
BCA2-8.1	296.6	6.4	0.05170	0.00071	0.04842	0.00089	0.34516	0.00802	0.572
BCA2-9.1	294.2	4.8	0.05378	0.00098	0.04733	0.00072	0.35092	0.00845	0.456
MFT1-1.1	302.5	7.7	0.05161	0.00092	0.04564	0.00107	0.32480	0.00960	0.569
MFT1-1.2	306.0	11.8	0.05312	0.00057	0.04835	0.00114	0.35417	0.00926	0.650
MFT1-10.1	304.2	9.2	0.05217	0.00021	0.04521	0.00114	0.32522	0.00842	0.704
MFT1-11.1	299.4	6.7	0.05247	0.00036	0.04794	0.00097	0.34684	0.00750	0.673

BCA-2- gabbro-diorite (39º4'5.9"N; 7º12'51"W); MFT-1- pinkish granite (39º04'4.5"N; 7º13'53"W)
SHRIMPTOOLS data processing; IBERSIMS laboratory, University of Granada, Spain
Errors are at one sigma level. The error in 206/238 averaging the standard has been already propagated. Th/U ratios are atomic (232/238), not in weight
Point-to point errors, calculated on replicates of the TEMORA standard, are: 0.36% for $^{206}Pb/^{238}U$, and 0.32% for $^{207}Pb/^{206}Pb$

TABLE 1. (Cont.)

	204-corrected isotope ratios								
id	**$^{208}Pb/^{232}Th$**	**±err**	**$^{207}Pb/^{206}Pb$**	**±err**	**$^{206}Pb/^{238}U$**	**±err**	**$^{207}Pb/^{235}U$**	**±err**	**rho_4cor**
MFT1-12.1	353.5	5.1	0.05088	0.00088	0.04748	0.00065	0.33312	0.00745	0.438
MFT1-13.1	292.7	5.4	0.05247	0.00046	0.04659	0.00074	0.33708	0.00626	0.619
MFT1-14.1	185.2	14.2	0.05203	0.00091	0.04334	0.00230	0.31090	0.01739	0.682
MFT1-15.1	292.5	6.2	0.05095	0.00055	0.04697	0.00089	0.32999	0.00730	0.618
MFT1-16.1	439.2	36.7	0.05279	0.00022	0.04361	0.00160	0.31740	0.01178	0.712
MFT1-17.1	306.0	5.2	0.05113	0.00117	0.04792	0.00080	0.33785	0.00966	0.420
MFT1-18.1	285.6	9.2	0.05238	0.00064	0.04437	0.00140	0.32045	0.01089	0.667
MFT1-18.2	264.2	13.6	0.05488	0.00348	0.03029	0.00135	0.22921	0.01778	0.414
MFT1-19.1	335.8	9.7	0.05016	0.00129	0.04746	0.00136	0.32819	0.01271	0.533
MFT1-19.2	676.9	20.4	0.05629	0.00475	0.03956	0.00103	0.30706	0.02715	0.212
MFT1-20.1	294.6	14.5	0.05343	0.00050	0.04528	0.00182	0.33362	0.01381	0.699
MFT1-21.1	282.6	7.8	0.04636	0.00103	0.04597	0.00114	0.29384	0.00987	0.534
MFT1-22.1	309.5	8.8	0.05192	0.00067	0.04815	0.00138	0.34471	0.01090	0.652
MFT1-23.1	1201.7	145.9	0.04393	0.04807	0.04702	0.00244	0.28483	0.31201	0.034
MFT1-24.1	298.2	6.8	0.05274	0.00028	0.04780	0.00105	0.34761	0.00795	0.692
MFT1-24.2	901.5	28.4	0.04949	0.00702	0.04589	0.00109	0.31310	0.04507	0.119
MFT1-25.1	308.5	6.3	0.05141	0.00059	0.04765	0.00072	0.33773	0.00651	0.562
MFT1-3.1	494.1	59.5	0.05420	0.00429	0.03671	0.00162	0.27435	0.02487	0.350
MFT1-4.1	471.1	45.6	0.05581	0.00409	0.03475	0.00174	0.26742	0.02377	0.405
MFT1-5.1	314.6	13.8	0.05354	0.00059	0.05056	0.00203	0.37325	0.01557	0.692
MFT1-6.1	307.2	5.5	0.05140	0.00063	0.04748	0.00081	0.33650	0.00716	0.577
MFT1-7.1	364.1	10.0	0.05213	0.00122	0.04654	0.00125	0.33452	0.01202	0.540
MFT1-8.1	315.1	9.9	0.05158	0.00044	0.04747	0.00144	0.33762	0.01068	0.689
MFT1-8.2	520.2	69.7	0.05850	0.00030	0.08680	0.00862	0.70014	0.06965	0.719
MFT1-9.1	329.8	13.8	0.05323	0.00138	0.04785	0.00171	0.35119	0.01554	0.580

BCA-2- gabbro-diorite (39º4'5.9"N; 7º12'51"W); MFT-1- pinkish granite (39º04'4.5"N; 7º13'53"W)
SHRIMPTOOLS data processing; IBERSIMS laboratory, University of Granada, Spain
Errors are at one sigma level. The error in 206/238 averaging the standard has been already propagated. Th/U ratios are atomic (232/238), not in weight
Point-to point errors, calculated on replicates of the TEMORA standard, are: 0.36% for $^{206}Pb/^{238}U$, and 0.32% for $^{207}Pb/^{206}Pb$

TABLE 1. (Cont.)

										204-corrected ages (Ma)	
id	**$^{208}Pb/^{232}Th$**	**±err**	**$^{207}Pb/^{206}Pb$**	**±err**	**$^{206}Pb/^{238}U$**	**±err**	**$^{207}Pb/^{235}U$**	**±err**	**% discord.**	**$^{208}Pb/^{232}Th$**	**±err**
BCA2-1.1	0.01392	0.00057	0.0	0.0	315.1	5.5	261.5	16.1	-20.4	279.3	11.3
BCA2-10.1	0.01436	0.00029	181.5	74.8	296.2	4.2	283.7	9.0	-4.4	288.1	5.7
BCA2-11.1	0.01536	0.00011	298.1	22.6	309.9	3.4	308.5	4.1	-0.4	308.1	2.2
BCA2-12.1	0.01381	0.00030	152.7	75.8	292.5	5.4	277.4	9.3	-5.4	277.1	5.9
BCA2-13.1	0.01282	0.00189	0.0	250.9	309.2	5.7	252.2	53.0	-22.6	257.5	37.8
BCA2-14.1	0.01440	0.00035	260.3	81.6	287.4	7.9	284.4	11.5	-1.0	288.9	7.0
BCA2-15.1	0.01563	0.00049	453.1	68.6	304.8	5.3	322.6	10.1	5.6	313.4	9.8
BCA2-16.1	0.01385	0.00036	0.0	160.5	298.9	5.0	275.9	8.9	-8.4	278.0	7.2
BCA2-17.1	0.01023	0.00032	259.7	96.4	248.2	4.4	249.3	10.5	0.4	205.7	6.5
BCA2-18.1	0.01039	0.00450	0.0	398.7	297.6	10.0	167.9	164.6	-77.2	208.9	90.3
BCA2-19.1	0.01524	0.00023	332.5	63.8	296.7	4.7	300.7	8.6	1.4	305.7	4.5
BCA2-2.1	0.01460	0.00034	110.5	82.4	309.1	4.8	287.0	9.9	-7.8	292.9	6.7
BCA2-20.1	0.01431	0.00036	131.3	103.2	303.9	3.2	284.8	11.6	-6.8	287.2	7.1
BCA2-21.1	0.01456	0.00015	337.9	39.8	300.1	5.3	304.5	6.8	1.4	292.1	3.1
BCA2-22.1	0.01556	0.00025	364.9	56.0	311.6	3.1	318.0	7.5	2.0	312.1	5.0
BCA2-23.1	0.01454	0.00039	169.3	106.0	297.9	4.8	283.8	12,4	-5.0	291.7	7.8
BCA2-24.1	0.01289	0.00067	0.0	0.0	312.2	3.4	261.5	14.1	-19.4	258.8	13.5
BCA2-3.1	0.01561	0.00042	259.3	77.8	317.2	5.7	310.3	10.5	-2.2	313.1	8.4
BCA2-4.1	0.01498	0.00050	335.9	102.6	303.0	4.5	306.8	13.1	1.2	300.5	10.0
BCA2-5.1	0.01485	0.00039	198.5	84.6	304.9	5.3	292.9	10.6	-4.0	297.9	7.8
BCA2-6.1	0.01488	0.00021	216.5	65.6	298.0	4.4	289.0	8.3	-3.2	298.5	4.1
BCA2-7.1	0.01509	0.00022	337.7	36.6	306.3	5.0	310.0	6.3	1.2	302.6	4.4
BCA2-8.1	0.01467	0.00018	272.3	30.8	304.8	5.5	301.1	6.1	-1.2	294.3	3.5
BCA2-9.1	0.01493	0.00015	361.7	40.8	298.1	4.5	305.4	6.4	2.4	299.5	2.9
MFT1-1.1	0.01422	0.00030	268.1	40.2	287.7	6.6	285.6	7.4	-0.8	285.3	6.0
MFT1-1.2	0.01500	0.00047	334.1	24.0	304.4	7.0	307.9	7.0	1.2	300.9	9.4
MFT1-10.1	0.01366	0.00014	292.9	9.0	285.1	7.1	285.9	6.5	0.2	274.1	2.9
MFT1-11.1	0.01486	0.00014	306.1	15.4	301.9	6.0	302.3	5.6	0.2	298.1	2.8

BCA-2- gabbro-diorite (39º4'5.9"N; 7º12'51"W); MFT-1- pinkish granite (39º04'4.5"N; 7º13'53"W)
SHRIMPTOOLS data processing; IBERSIMS laboratory, University of Granada, Spain
Errors are at one sigma level. The error in 206/238 averaging the standard has been already propagated. Th/U ratios are atomic (232/238), not in weight
Point-to point errors, calculated on replicates of the TEMORA standard, are: 0.36% for $^{206}Pb/^{238}U$, and 0.32% for $^{207}Pb/^{206}Pb$

TABLE 1. (Continued)

					204-corrected ages (Ma)						
id	**$^{208}Pb/^{232}Th$**	**±err**	**$^{207}Pb/^{206}Pb$**	**±err**	**$^{206}Pb/^{238}U$**	**±err**	**$^{207}Pb/^{235}U$**	**±err**	**% discord.**	**$^{208}Pb/^{232}Th$**	**±err**
MFT1-12.1	0.01510	0.00032	235.7	39.6	299.0	3.9	291.9	5.6	-2.4	302.9	6.5
MFT1-13.1	0.01433	0.00017	306.1	20.0	293.5	4.5	295.0	4.8	0.6	287.5	3.4
MFT1-14.1	0.00717	0.00050	286.7	39.6	273.5	14.2	274.9	13.6	0.6	144.4	10.1
MFT1-15.1	0.01439	0.00017	238.7	24.6	295.9	5.5	289.6	5.6	-2.2	288.7	3.4
MFT1-16.1	0.01794	0.00080	319.7	9.4	275.2	9.9	279.9	9.1	1.6	359.4	15.9
MFT1-17.1	0.01511	0.00033	246.9	52.0	301.7	4.9	295.5	7.3	-2.0	303.2	6.6
MFT1-18.1	0.01391	0.00020	301.9	27.8	279.9	8.7	282.2	8.4	0.8	279.2	4.0
MFT1-18.2	0.00521	0.00041	407.3	135.8	192.4	8.5	209.5	14.7	8.2	105.0	8.3
MFT1-19.1	0.01449	0.00050	202.3	58.8	298.9	8.4	288.2	9.8	-3.8	290.8	10.1
MFT1-19.2	0.01505	0.00105	463.7	177.0	250.1	6.4	271.9	21.3	8.0	301.9	21.0
MFT1-20.1	0.01477	0.00034	347.3	20.8	285.5	11.2	292.3	10.5	2.4	296.3	6.7
MFT1-21.1	0.01226	0.00036	0.0	0.0	289.7	7.0	261.6	7.8	-10.8	246.2	7.2
MFT1-22.1	0.01513	0.00021	281.9	29.2	303.2	8.5	300.7	8.2	-0.8	303.6	4.2
MFT1-23.1	0.01650	0.01405	0.0	1467.3	296.2	15.0	254.5	282.5	-16.4	330.8	281.3
MFT1-24.1	0.01480	0.00010	317.7	11.8	301.0	6.4	302.9	6.0	0.6	297.0	2.1
MFT1-24.2	0.01393	0.00190	170.9	301.6	289.2	6.7	276.6	35.5	-4.6	279.6	38.0
MFT1-25.1	0.01512	0.00027	259.1	26.2	300.1	4.4	295.4	4.9	-1.6	303.3	5.5
MFT1-3.1	0.01153	0.00333	379.3	168.8	232.4	10.1	246.2	20.0	5.6	231.7	66.7
MFT1-4.1	0.01333	0.00197	444.9	155.2	220.2	10.8	240.6	19.2	8.4	267.7	39.3
MFT1-5.1	0.01575	0.00019	351.9	24.6	317.9	12.4	322.1	11.6	1.4	315.9	3.7
MFT1-6.1	0.01443	0.00015	258.7	27.8	299.0	4.9	294.5	5.4	-1.6	289.5	3.1
MFT1-7.1	0.01503	0.00042	291.1	52.8	293.3	7.8	293.0	9.2	-0.2	301.5	8.4
MFT1-8.1	0.01388	0.00020	266.9	19.2	299.0	8.9	295.4	8.2	-1,2	278.7	4.0
MFT1-8.2	0.02540	0.00037	548.7	11.0	536.6	51.3	538.9	42.5	0.4	506.9	7.2
MFT1-9.1	0.01423	0.00032	338.5	57.8	301.3	10.5	305.6	11.7	1.4	285.6	6.3

BCA-2- gabbro-diorite (39º4'5.9"N; 7º12'51"W); MFT-1- pinkish granite (39º04'4.5"N; 7º13'53"W)
SHRIMPTOOLS data processing; IBERSIMS laboratory, University of Granada, Spain
Errors are at one sigma level. The error in 206/238 averaging the standard has been already propagated. Th/U ratios are atomic (232/238), not in weight
Point-to point errors, calculated on replicates of the TEMORA standard, are: 0.36% for $^{206}Pb/^{238}U$, and 0.32% for $^{207}Pb/^{206}Pb$